R-896

LARGE SPACE TELESCOPE CONTROL MOMENT GYRO TEST PROGRAM

by

Eugene Salamin
George J. Bukow

July 1975

The Charles Stark Draper Laboratory, Inc.
Cambridge, Massachusetts 02139

R-896

LARGE SPACE TELESCOPE CONTROL MOMENT GYRO TEST PROGRAM

by

Eugene Salamin
George J. Bukow

July 1975

FINAL REPORT
NAS 8-30249

The Charles Stark Draper Laboratory, Inc.
Cambridge, Massachusetts 02139

Approved: for N. E. Sears

ACKNOWLEDGMENT

This report was prepared by The Charles Stark Draper Laboratory, Inc. under Contract NAS 8-30249 with the NASA Marshall Space Flight Center under the direction of Gerald Nurre, George Doane, and Gene Fikes.

Among the Draper Laboratory personnel who contributed to this effort were our project manager, Gerald Ouellette, our division leader, Jerold Gilmore, and staff engineers Francis Merenda, Dale Woodbury, and Stephen Helfant. Mr. Merenda and Mr. Woodbury put in extensive efforts in the development and test of the electronics and instrumentation used in the test program. Mr. Merenda also ably handled the testing at Martin Company. Mr. Helfant and Mrs. Linda Willy were very helpful in preparing data presentations and the content of the final report.

We owe special thanks to the personnel of the Martin Company Inertial Gyro Laboratory, in particular Bud Gates, Norman Osborne, and Dale Wine for their close cooperation and ready assistance.

The publication of this report does not constitute approval by the National Aeronautics and Space Administration of the findings or the conclusions contained therein. It is published solely for the exchange and stimulation of ideas.

Prepared for George C. Marshall Space Flight Center
Marshall Space Flight Center, Alabama 35812

ABSTRACT

This final report describes in detail the underlying theory and design of test instrumentation and computer techniques used to determine the power spectral density (PSD) of the Draper Laboratory Third Generation Gyro. Acceptance test results on the completed instrument (instrument build funded in part under this program) are presented as well as composite PSD plots determined from data taken at both Draper Laboratory and at Martin Company, Denver. The measured RMS noise over the frequency band 0.0025 - 10 Hz was 0.012 arc seconds (at Draper Laboratory). Results obtained at Martin Company indicate an RMS noise of 0.009 arc seconds (0.05 - 10 Hz). The results obtained showed the TGG performance was close to the proposed LST requirements but that additional development work would be needed to reduce the TGG noise to within more desirable limits.

Table of Contents

List of Illustrations

List of Illustrations (Cont.)

CHAPTER 1

INTRODUCTION

The Large Space Telescope/Control Moment Gyro (LST/CMG) test program attempted to establish the capability of low noise inertial gyros in precision stabilization and control of space vehicles. The basic approach used was two-fold:

1) Establish gyro noise characteristics (18 IRIG Mod D and the Third Generation Gyro (TGG)) in the 0.003 to 10Hz band.

2) Determine gyro performance when used as an integral part of a simulated LST fine pointing system.

The individual tasks included the setup and test of two 18 IRIG Mod D gyros in a back-to-back configuration, build and test (basic acceptance) a TGG from parts furnished GFE from the Air Force (SAMSO), establish TGG noise levels (at Draper Lab), and perform TGG noise measurements and LST system tests at the Martin Company in Denver, Colorado.

CHAPTER 2

DESCRIPTION OF TEST PROGRAM

1. 18 IRIG Back-to-Back Testing

The 18 IRIG Mod D gyro is a moderate performance rate integrating gyro designed and built at Draper Laboratory. It is a floated, viscous damped instrument with a gas bearing wheel, magnetic suspension, bridge type signal generator and soft iron torque generator.

Two 18 IRIG's were mounted in a common test fixture (input axes parallel) and instrumented as shown in Fig. 1. A brief description of the system shown in Fig. 1 is presented in the following paragraphs. A more detailed analysis of the electronics design and of the power spectral density (PSD) techniques used are presented in Chapters 4 and 5.

The outputs from the two 18 IRIG's were amplified and coupled through split winding transformers. The difference signal shown is the algebraic difference of the output signals from the two gyros. This signal was filtered, demodulated, and processed using PSD techniques.

The difference signal eliminated any common mode output exhibited by the two gyros. The prime common mode signal was expected to be ground motion inputs to the two gyros.

Also available for measurement and analysis were the individual gyro output signals. These signals were processed and compared to the difference output. The results obtained are discussed in Chapter 6.

2. TGG Tests

The Draper Lab TGG is a high performance, floated, viscous damped, rate integrating gyro. The instrument has extremely low drift and low noise and was considered an excellent candidate for the LST/CMG program. The TGG employs a gas bearing wheel, bridge type signal generator, and a soft iron torque generator.

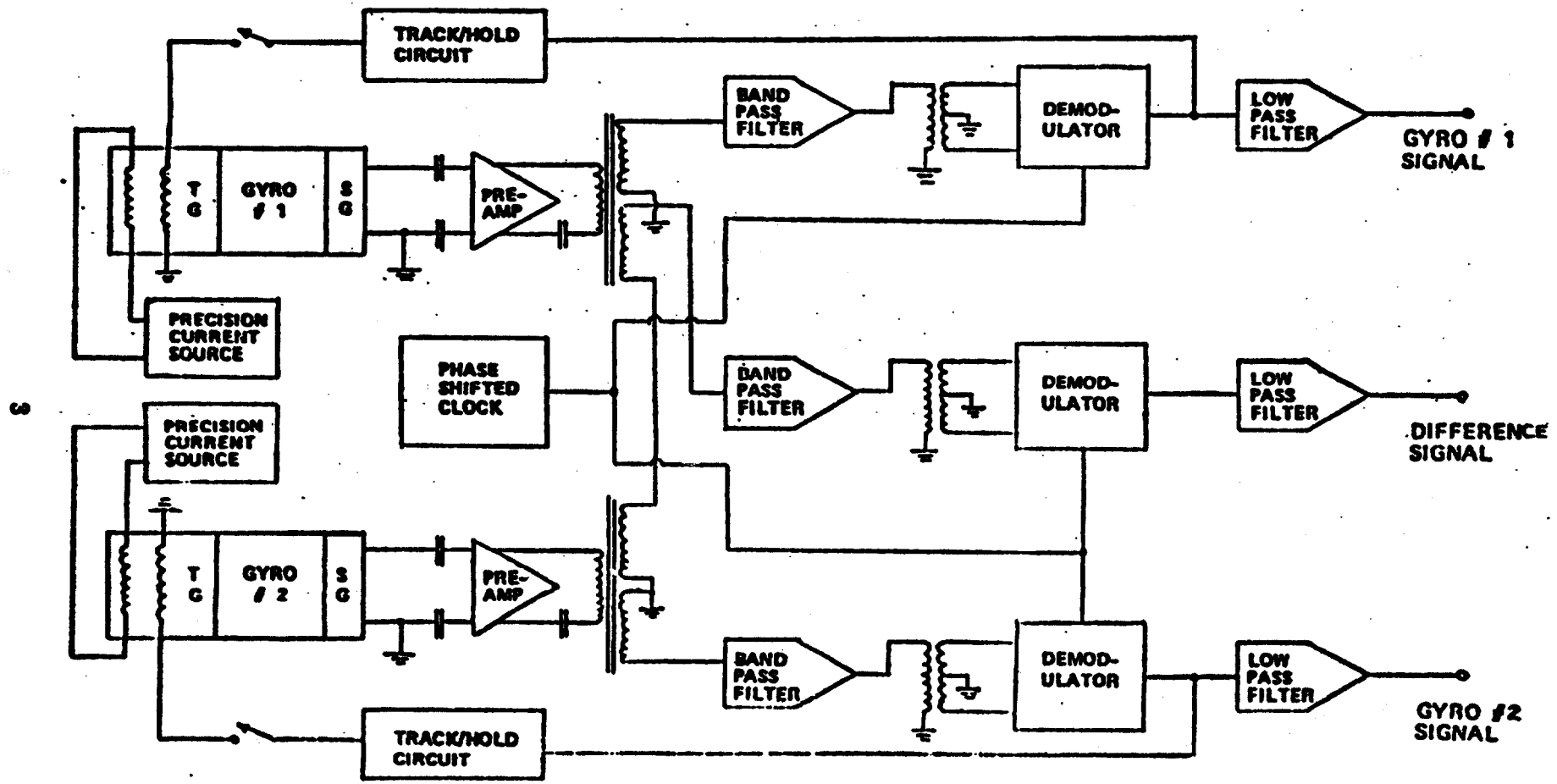

Fig. 1 LST/CMG Test, Gyro Noise Measurement System

The basic acceptance test results for the TGG are presented in Chapter 3. After passing the basic acceptance test, the TGG was integrated with a system configuration similar to that employed with the 18 IRIG's. No back-to-back testing (TGG with 18 IRIG) was performed due to the high noise measured with the 18 IRIG (see Chapter 6).

3. TGG Noise Measurements

Noise measurements were obtained for the TGG at Draper Laboratory and at the Martin Company, Denver, Colorado. Unfortunately, numerous computer related hardware and system software problems limited the overall success of the program and a complete characterization of the TGG noise could not be obtained during the initial contract period.

Draper Laboratory requested a contract extension to allow Draper engineers the use of the contract deliverables on a separate program. During the extension period additional data was obtained at Draper Laboratory which allowed a complete spectrum to be obtained for the TGG. This data is presented in Fig. 23 of Chapter 6. The RMS noise obtained in the band 0.0025 - 10 Hz was 0.012 arc second.

Per NASA direction, the Martin test effort concentrated on obtaining a comprehensive TGG noise characterization. Due to lack of adequate funding the testing of the TGG on the Martin fine pointing simulator was not accomplished.

CHAPTER 3

TGG ACCEPTANCE TEST SUMMARY

Standard acceptance tests on TGG-G1A-221x were completed on 4/12/74 prior to delivery of the instrument to the LST/CMG Program. Test results obtained are tabulated in Table 1 below. In addition to those results listed in Table 1, the following tests were performed and found to be within specified limits: thermal cycling (320^{o} - 155^{o}F), insulation resistance, signal generator and torque generator phasing, magnetic suspension tuning, float freedom, axial and radial centering, unbalance coefficient.

TABLE 1

TGG ACCEPTANCE TEST RESULTS

	Numerical Value	Units
Float stops	+4.0 - 4.7	mrad
Signal generator null voltage	3.0	mV
Flotation temperature	134.7	^{o}F
Gyro gain	130	mV/mrad
Torque generator sensitivity (per winding)	0.050	dyn-cm/$\overline{mA}^2$
Signal generator sideband noise (due to wheel unbalance)	0.11	mV (@533 Hz)
Total reaction torque	<0.22	dyn-cm
Wheel excitation voltage	45	V
Wheel operating power	10.8	W
Average wheel power sensitivity	0.015	deg/h/W
Average wheel voltage sensitivity	0.003	deg/h/V
Wheel run-up time	30	seconds
Wheel run-down time	110	seconds

CHAPTER 4

GYRO NOISE MEASUREMENT ELECTRONICS

1. General Description (Fig. 2).

The SG output of each gyro is amplified with a low noise preamp. By coupling the preamp outputs through split winding transformers, we obtain individual gyro signals and also a difference signal.

A band pass filter provides selective amplification at the carrier frequency, and then a phase sensitive demodulator converts the signal to dc. A low pass filter provides the output for digitization by an A-D converter.

The TGG and the 18 Mod D have, in effect, two torque generators. One TG, driven from a precision constant current source, is used to cancel the major portion of earth rotation and gyro drift. The other TG is used in one of two modes:

(1) analog rebalance loop, or
(2) constant dc current.

When operating in mode (1), a track/hold circuit steps the output of a D-A converter to follow the analog torque current. When the tracking circuit has settled, mode (2) provides a dc current at the proper value to prevent the float from drifting away from null. This technique allows automatic compensation for gyro drift.

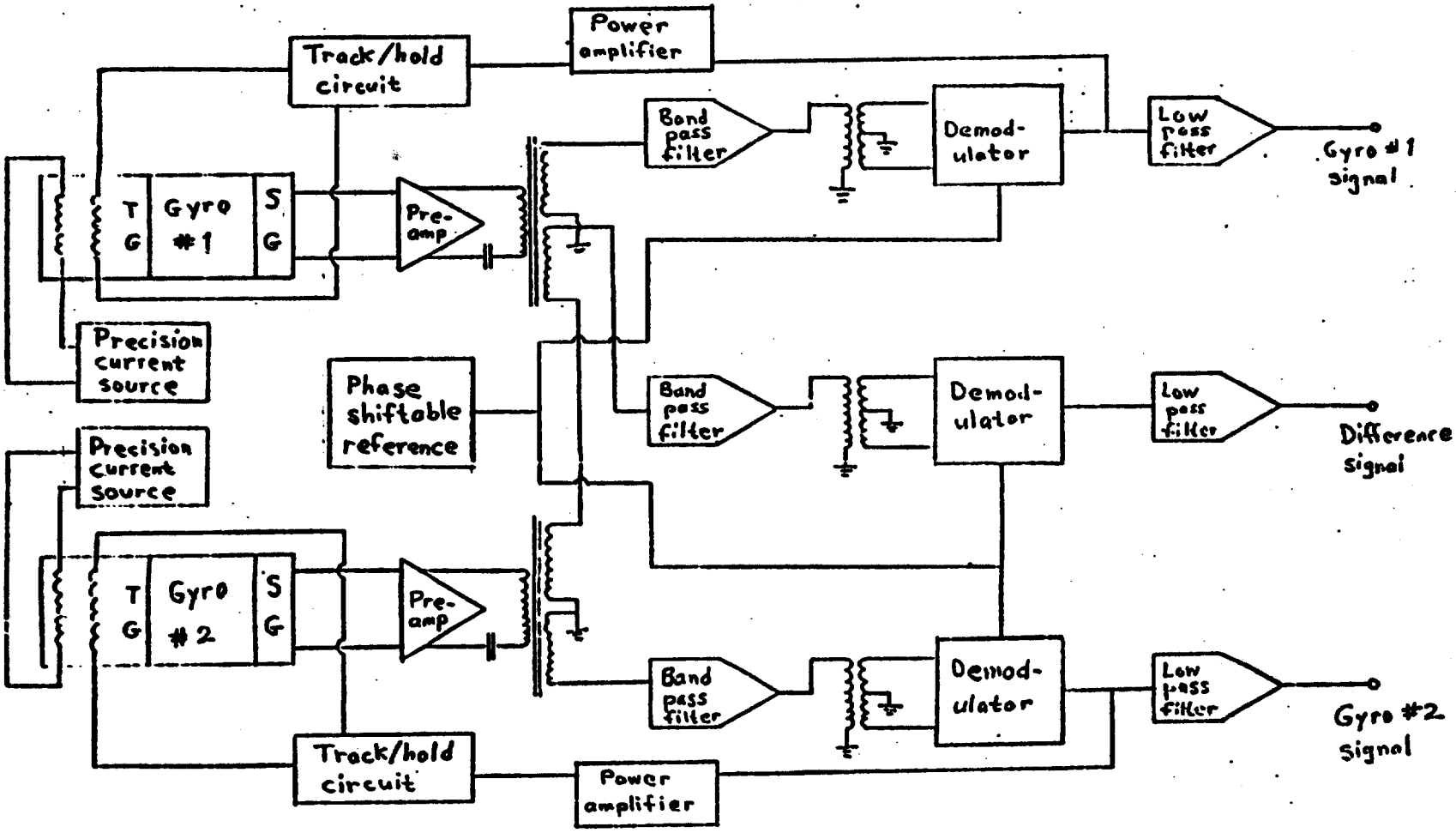

Fig. 2 Gyro Noise Measurement System

The following gyro parameters will be used below [refs. 1, 2].

	TGG	18 mod D	units
gyro gain	1.2	0.516	
SG sensitivity	15	6.6	V(RMS)/rad
SG resistance at 6400 Hz	66	59	Ω
float time constant	750	416	μsec

2. Preamp (figure 3).

The preamp uses an LM381A integrated circuit op-amp [refs. 3, 4]. This amplifier, marketed for high fidelity applications, has a noise voltage of 5 nV/ $\sqrt{\text{Hz}}$ and a noise current of 0.3 pA/ $\sqrt{\text{Hz}}$ at the carrier frequency (6400 Hz).

The signal to noise ratio is maximum for a source impedance of 16700Ω, and this requires a 1:16 turns ratio transformer to couple the SG to the preamp. The most readily available transformers having this turns ratio also have so low a primary impedance that the SG would be excessively loaded. It was decided to postpone the purchase of a suitable transformer until its necessity is established. Failure to match impedances costs a loss of signal to noise ratio by a factor of 12.

Because of the differential configuration, the amplifier noise is multiplied by 2. Using the gyro gain and the untuned SG sensitivity, we find the angle equivalent amplifier noise to be 0.39 nrad/ $\sqrt{\text{Hz}}$ for the DSG and 2.1 nrad/$\sqrt{\text{Hz}}$ for the 18 mod D. For a 10 Hz bandwidth, the RMS noise would be 1.25 nrad and 6.6 nrad respectively.

The preamp gain is 200, a factor of 100 coming from the closed loop gain of the op-amp, and a factor of 2 coming from the output transformer.

The grounding scheme for the SG and preamp is shown in figure 4. The input is kept balanced for maximum common mode rejection.

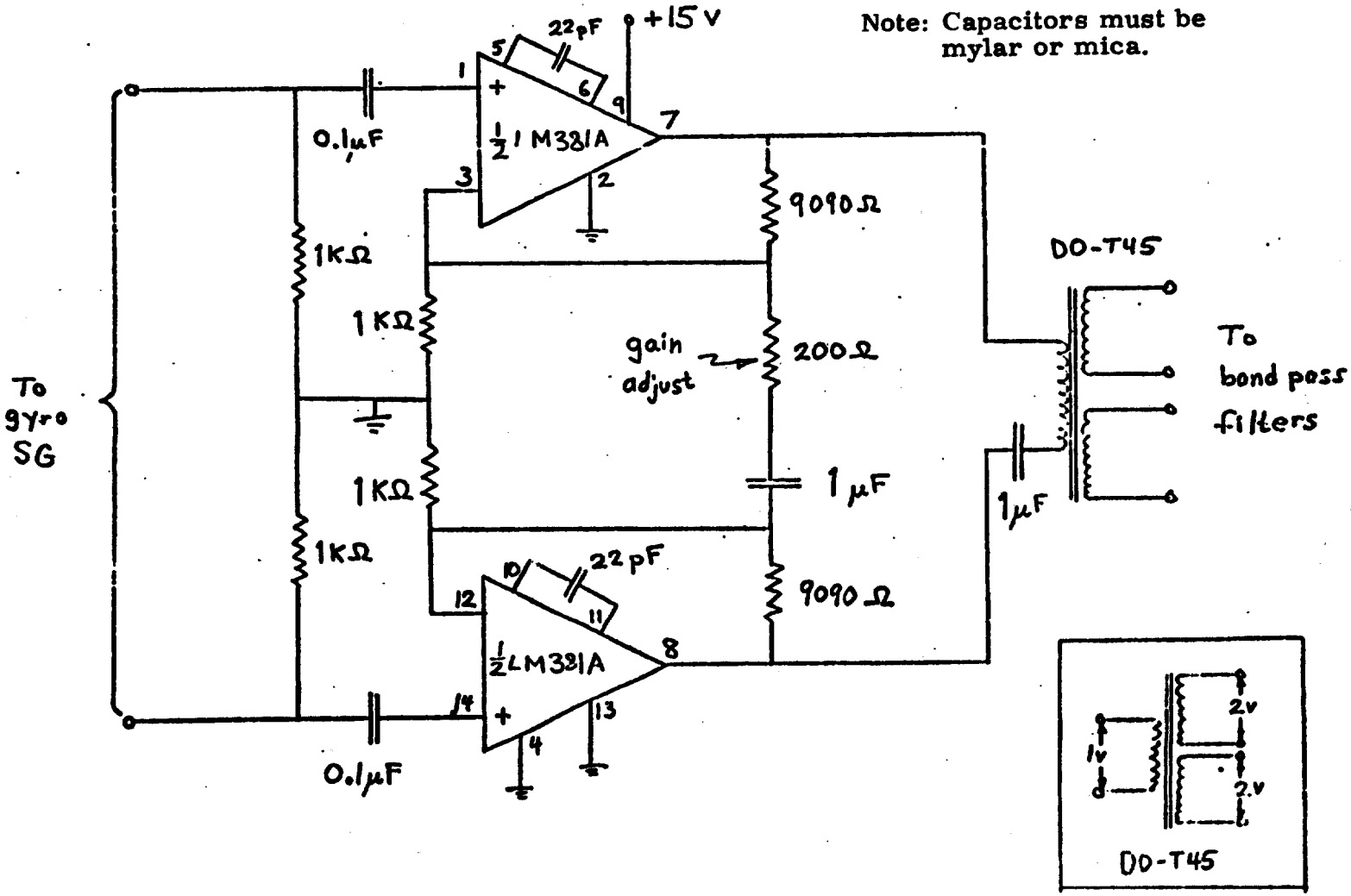

Fig. 3 Low Noise Preamplifier

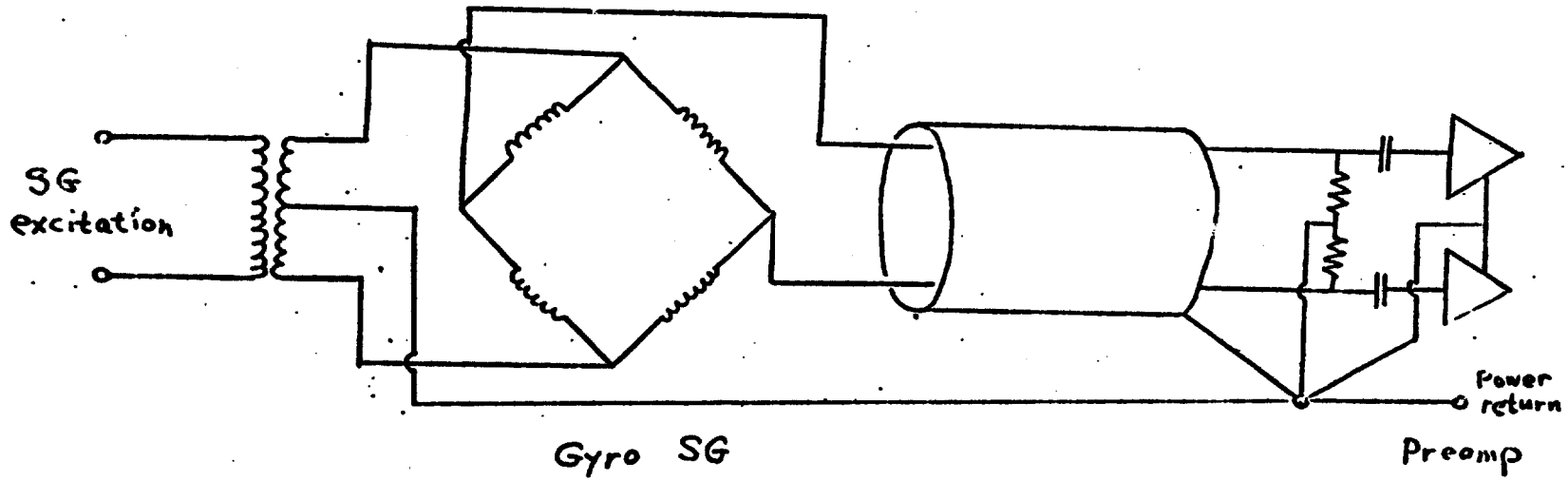

Fig. 4 Ground Scheme

3. Band Pass Filter (figure 5).

This filter is of the "negative immitance converter" type [ref. 5]. The transfer function is

$$G(S) = -G_0 \frac{(\omega_0/Q)\,S}{S^2 + (\omega_0/Q)S + \omega_0^2}, \qquad (1)$$

where $G_0 = 20$,

$$\omega_0 = 2\pi \times 6400 \text{ Hz}, \quad \text{and} \quad Q = (G_0+1)/2 = 10.5 .$$

This function is plotted in figures 6 and 7.

Let us derive the effect of the filter on the demodulated signal.

Signal: e^{st}

Carrier: $\cos \omega_0 t = \frac{1}{2}\left(e^{i\omega_0 t} + e^{-i\omega_0 t} \right)$

Modulate: $\frac{1}{2}\left(e^{(s+i\omega_0)t} + e^{(s-i\omega_0)t} \right)$

Filter: $\frac{1}{2}\left[G(S+i\omega_0)\, e^{(s+i\omega_0)t} + G(S-i\omega_0)\, e^{(s-i\omega_0)t} \right]$

Demodulate and normalize: $\frac{1}{2}\left[G(S+i\omega_0) + G(S-i\omega_0) \right] e^{st}$

Hence the effect on the float angle is given by the transfer function

$$H(s) = \frac{1}{2}\left[G(S+i\omega_0) + G(S-i\omega_0) \right] \qquad (2)$$

$$= \frac{1 + 2Q(S/\omega_0) + (S/\omega_0)^2 + Q(S/\omega_0)^3}{1 + 4Q(S/\omega_0) + (4Q^2+1)(S/\omega_0)^2 + 2Q(S/\omega_0)^3 + Q^2(S/\omega_0)^4} . \qquad (3)$$

This function is plotted figure 8.

4. Demodulator (figure 9).

The domodulator uses an AH0014 integrated circuit analog switch [refs. 3, 4] driven by a digitally phase shiftable reference square wave. The LM308A amplifier was selected for its low drift (5 μV/$^{\circ}$C).

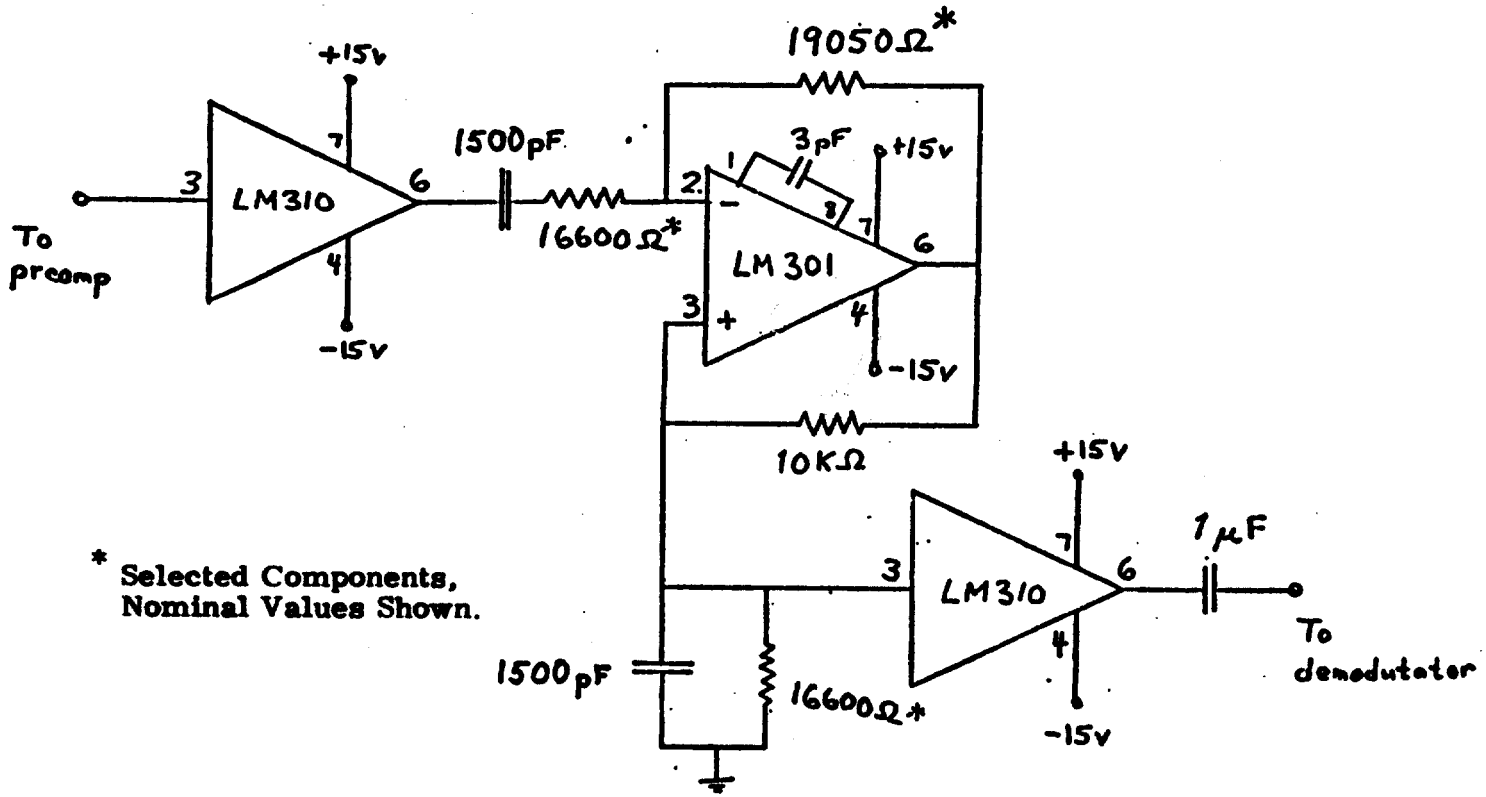

* Selected Components, Nominal Values Shown.

Fig. 5 Band Pass Filter

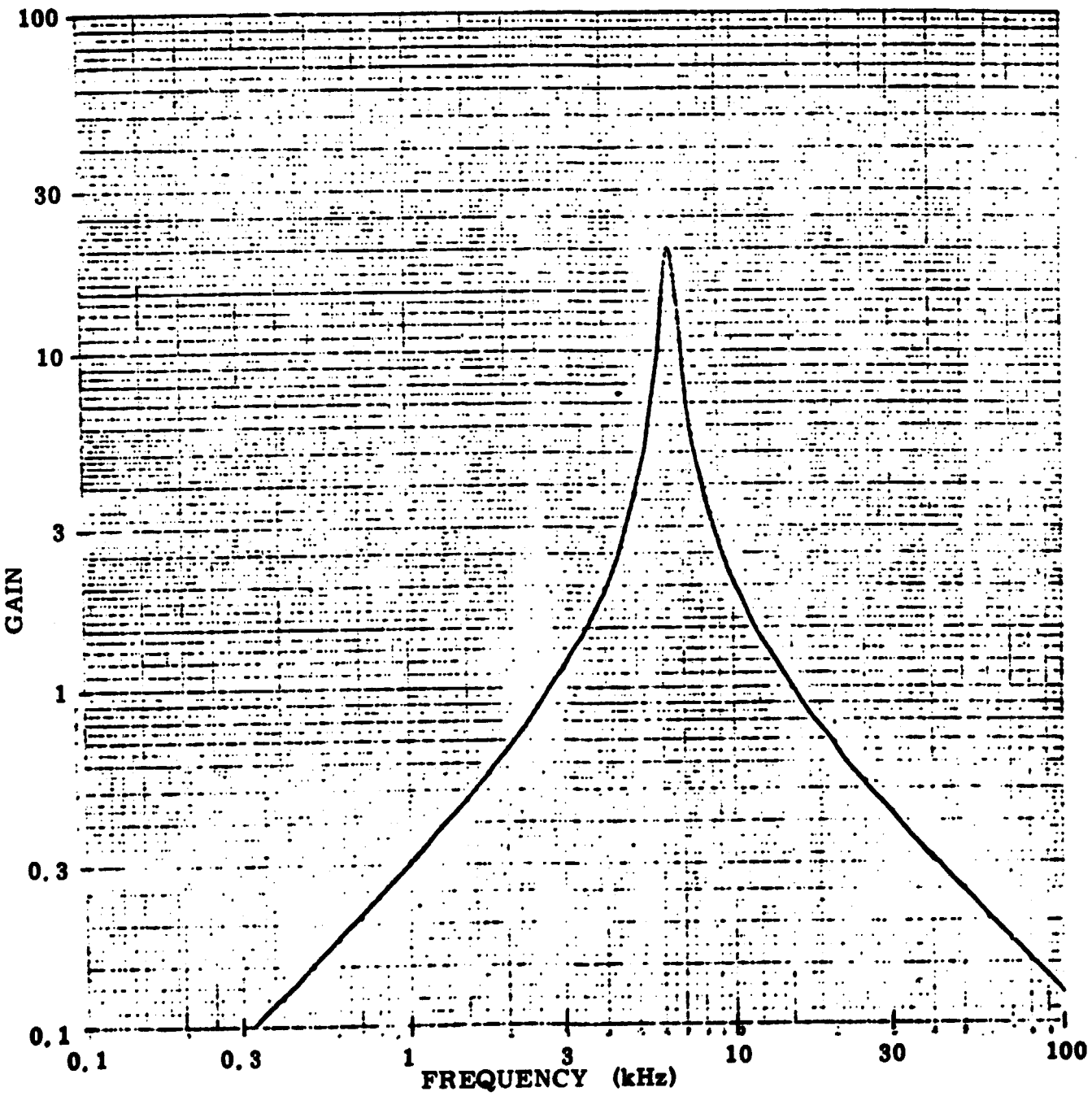

Fig. 6 Gain of Band Pass Filter

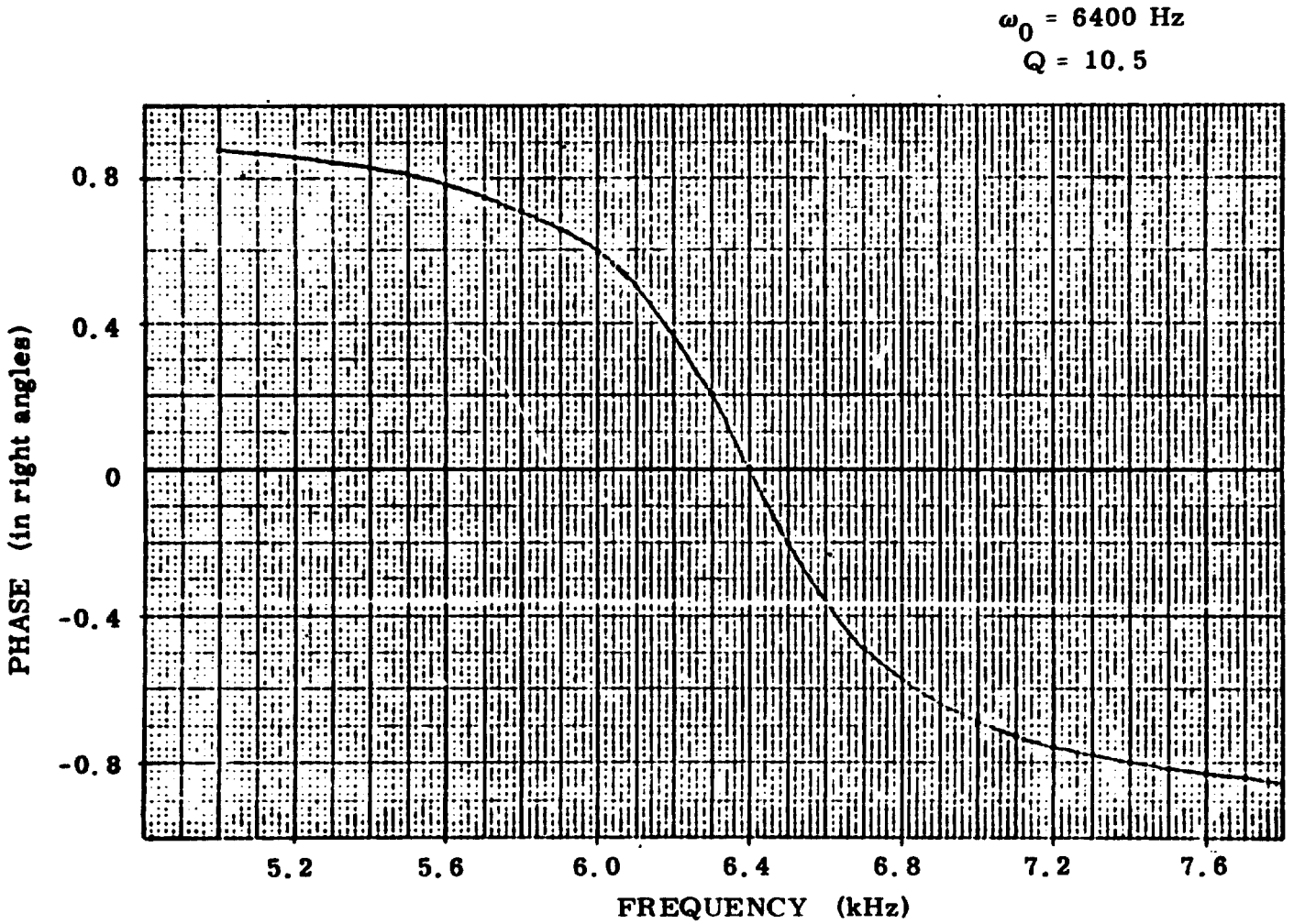

Fig. 7 Phase Response of Band Pass Filter

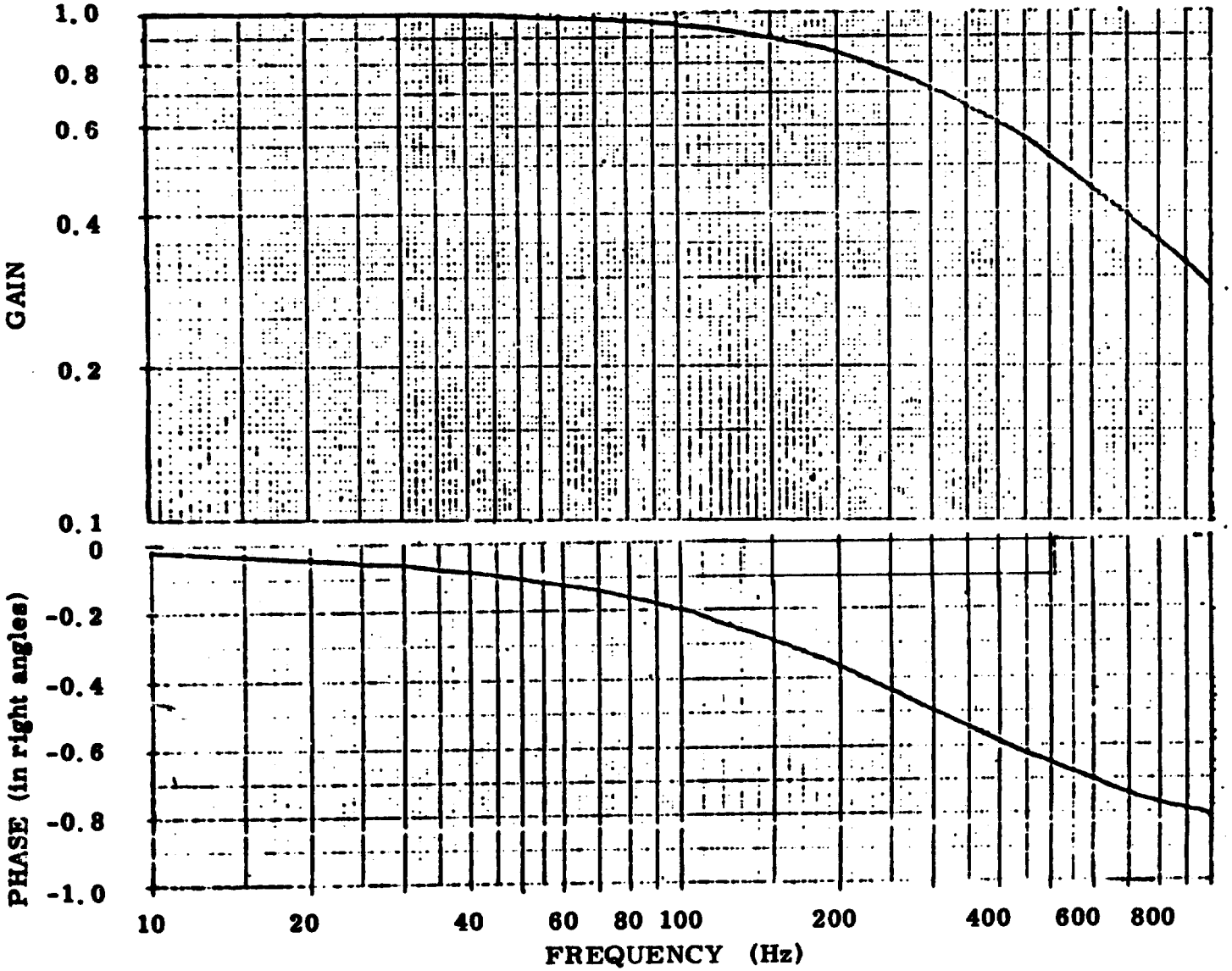

Fig. 8 Response of Bandpass Filter with Respect to Frequency of Demodulated Signal (Float Angle) Normalized to 1 at DC

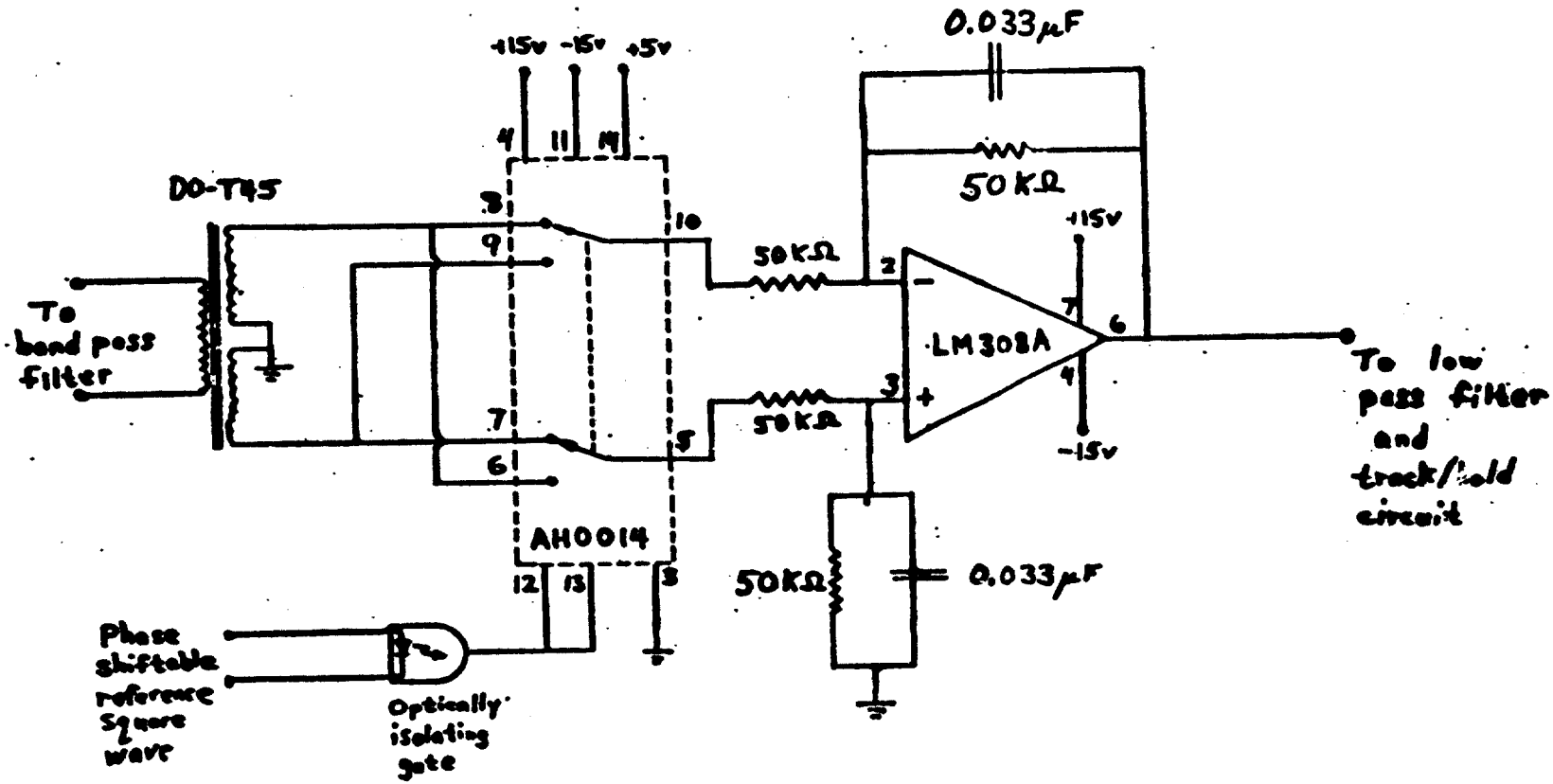

Fig. 9 Demodulator

The demodulator gain is considered in steps. First convert from RMS to zero-to-peak, giving a gain of $\sqrt{2}$. Going from single ended to differential through the input transformer gives a gain of.2. The amplifier has a gain of 1, but going from differential back to single ended through the amplifier gives a gain of 2. Also, there is a gain of $2/\pi$ in converting from zero-to-peak to average DC.

A ripple filter is included, and the overall transfer function is (for RMS input and DC output)

$$\frac{3.6}{s+\omega_1}, \qquad (4)$$

where $\omega_1 = 2\pi \times 100$ Hz.

5. Low Pass Filter (figure 10).

This two-pole filter is used to reduce aliasing. Its gain and cut-off frequency can easily be varied to suit test conditions. The transfer function is

$$\frac{G}{(s+\omega_2)^2}, \qquad (5)$$

where $\omega_2 = 2\pi \times 10$ Hz, and $G = 1$ for the DSG electronics and G = 10 for the 18 mod D electronics.

6. Power Amplifier (figure 11).

This amplifier has a transistor output stage to allow higher loads than an integrated circuit op-amp could tolerate. The gain and output resistor are chosen to give a good closed loop transient response and a good operating range between saturation points.

7. Track/Hold Circuit (figure 12).

This circuit contains a 16 bit digital to analog converter (DAC) driven by an up-down counter. Although 16 bits is more than we need, the concomitant stability of its output motivates the choice of this DAC. It has a current source output in the range of ±1 mA capable of driving up to 1000 Ω. A 3PDT switch selects either track mode or hold mode.

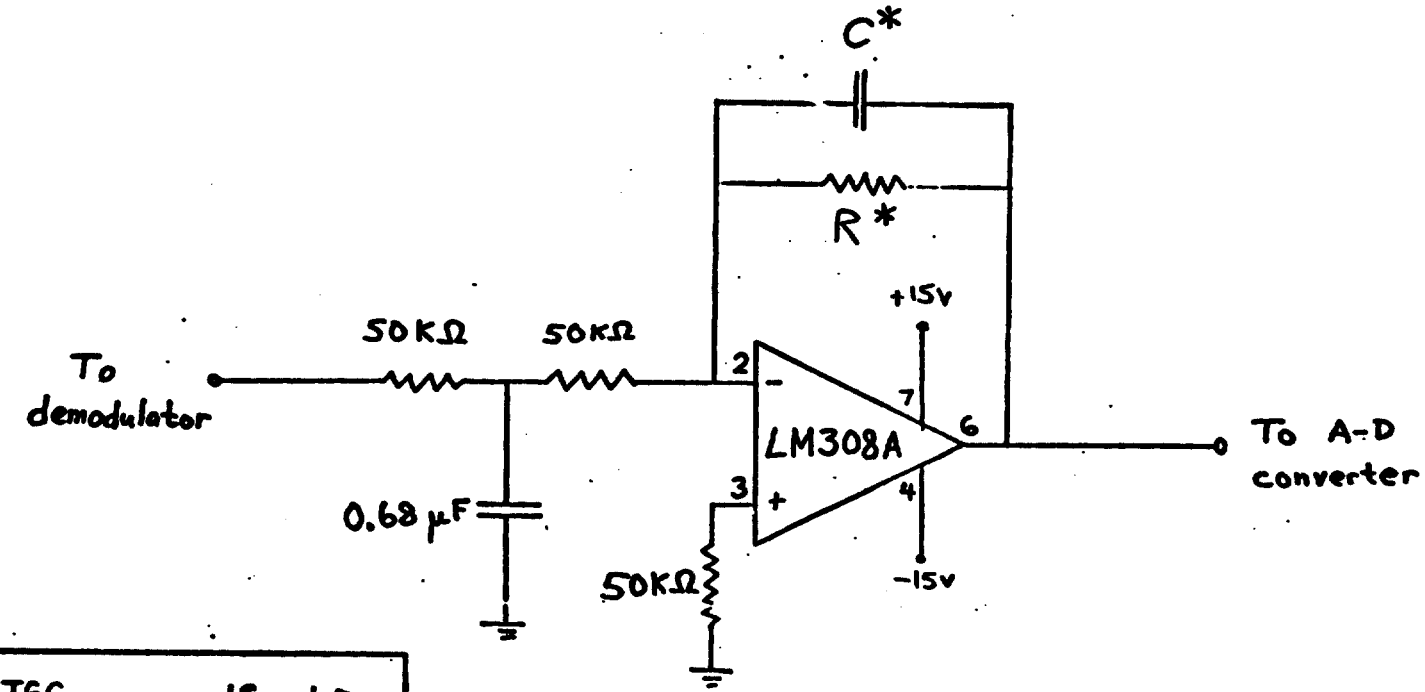

*	TGG	18 mod D
R	100 KΩ	1 MΩ
C	0.17 μF	0.017 μF

Fig. 10 Low Pass Filter

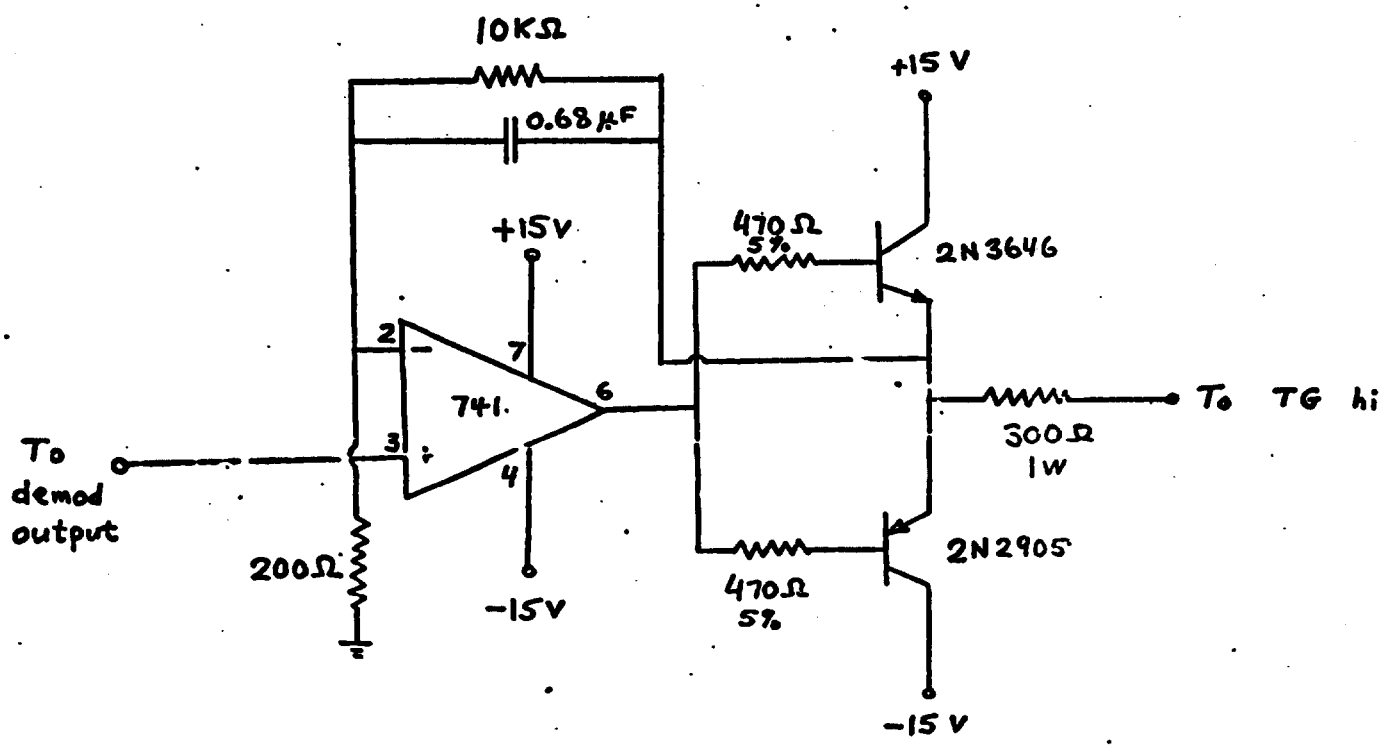

Fig. 11 Power Amplifier

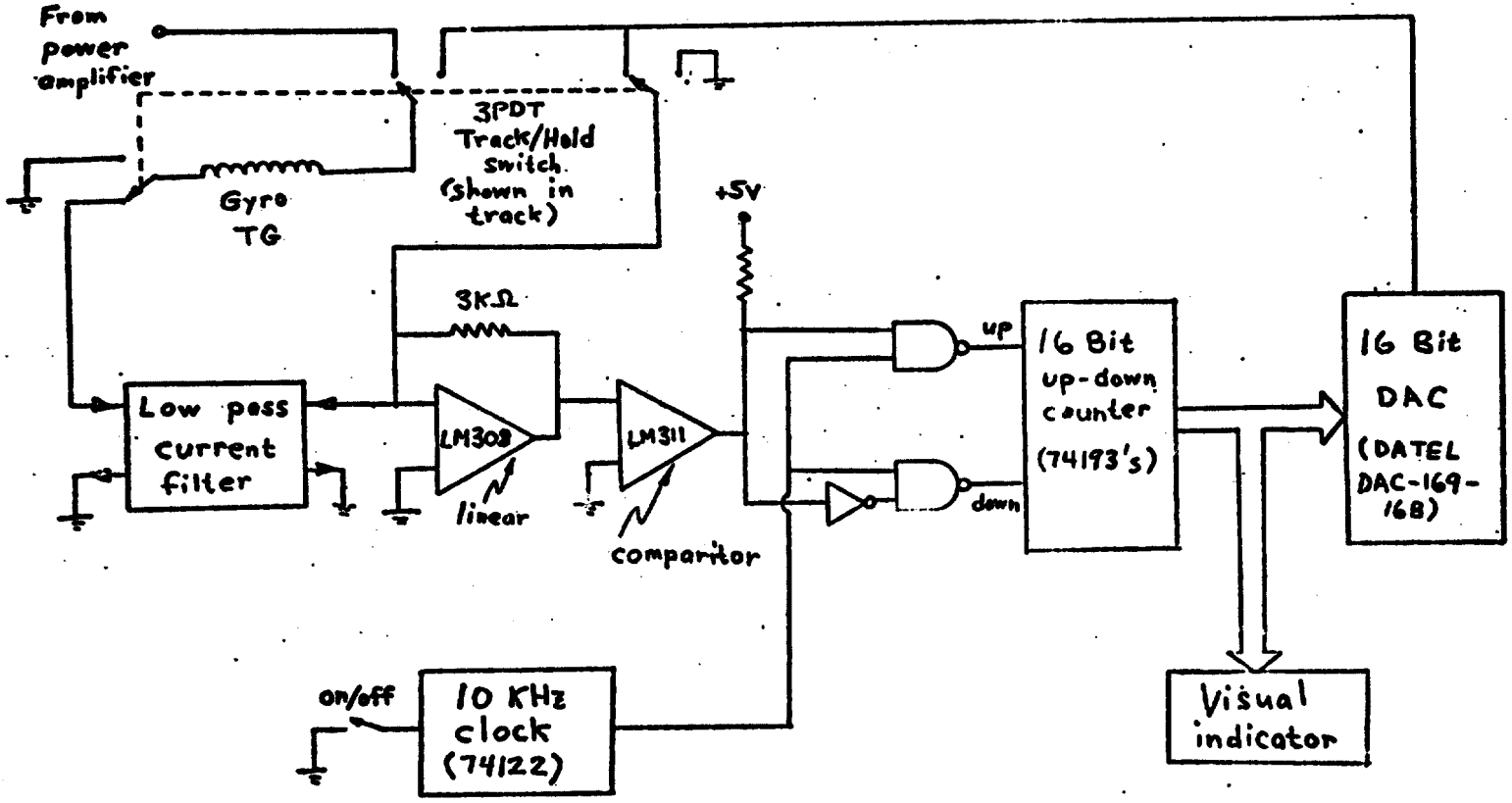

Fig. 12 Track/Hold Circuit

7.1 Track Mode.

The TG is placed into an analog rebalance loop. An inverting low pass current filter (figure 13) averages the TG current with a 20 second time constant. The difference between the average TG current and the DAC current is the error input to the tracking loop.

The error current is converted to voltage. The comparitor senses the sign of the error and steers the clock pulses into the up or down inputs of the counter so as to drive the error towards zero.

7.2 Hold Mode.

Constant current from the DAC flows throught the TG. The clock must be turned off before switching into hold mode.

8. TG Configurations.

8.1 The 18 IRIG mod D Gyro.

The TG configuration is shown in figure 14. The torque expressed as angular velocity is [ref. 2, supplemented with communications from the gyro designers]

$$\omega = \left(0.45 \frac{\mu rad/sec}{mA^2}\right) I_p (I_{s1} + I_{s2}). \qquad (6)$$

With ω=49 μrad/sec, the vertical component of earth rotation at CSDL, and with $I_{s2} = 0$, we get $I_p = I_{s1} = 10.4$ mA, which is supplied by a precision constant current source. DAC current I_{s2} is then applied with sensitivity 4.7 (μrad/sec)/mA. In hold mode the available current varies over a range of 2 mA, so the range of the track/hold circuit is 9.4 μrad/sec.

8.2 Third Generation Gyro

The TG configuration is shown in figure 15. The torque expressed as angular velocity is [ref. 1]

$$\omega = \left(0.095 \frac{\mu rad/sec}{mA^2}\right)\left[(I_{PO} + I_{SO})^2 - (I_{PE} + I_{SE})^2\right]. \qquad (7)$$

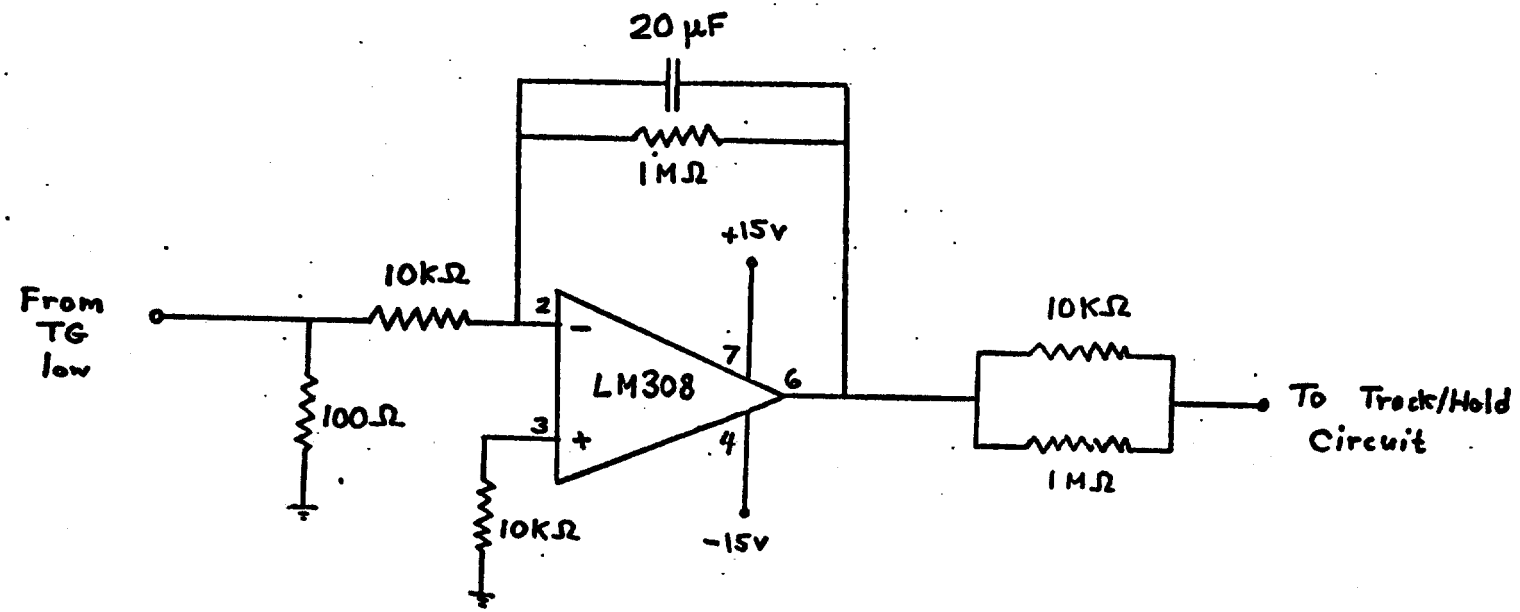

Fig. 13 Low Pass Current Filter

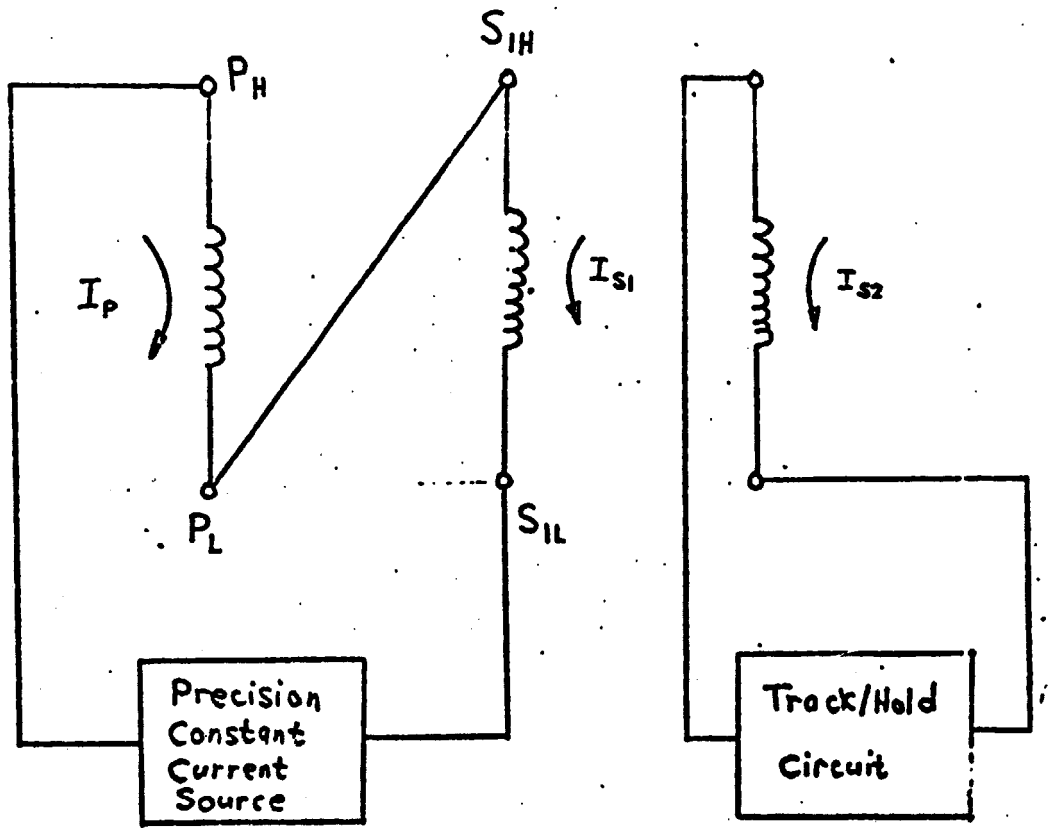

Fig. 14 Torque Winding Configuration for 18 IRIG Mod D Gyro with Microsyn Torquer

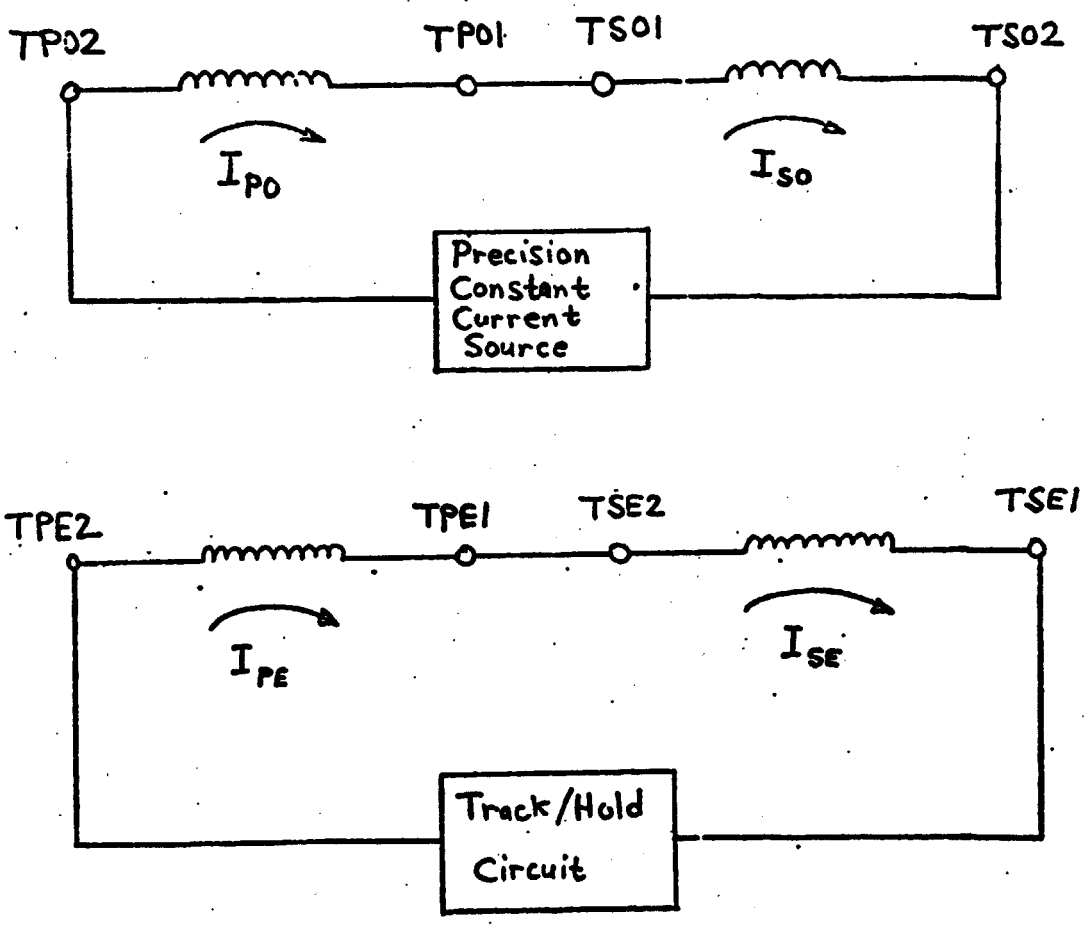

Fig. 15 Torque Winding Configuration for the TGG

With $I_{PE} = I_{SE} = 0.7$ mA and $\omega = 49$ μrad/sec, we get $I_{PO} = I_{SO} = 11.4$ mA, which is supplied by a precision constant current source. Then $I_{PE} = I_{SE}$ is supplied by the DAC. Since the DAC current is 0 to 1 mA, we get a track/hold range of 0.38 μrad/sec.

9. Preamp Gain Adjustment

In the dual gyro configuration, the gains of the two preamps must be adjusted so that the difference channel output shows no response to motion. This adjustment requires that the preamp outputs be in phase. SG tuning capacitors were not used because resonant circuits have rapidly varying phase shifts. There is no objection to the use of a tuning capacitor in the single gyro configuration.

Unfortunately, the LM381A preamp requires a capacitor for proper operation [ref. 4], and this introduces a phase shift. We have achieved an uncancelled motion sensitivity of 10 percent and expect to do better.

10. Measurement System Gain and Transfer Function.

The transfer function of the measurement system can be computed by multiplying together its components: gyro transfer function, which includes the float time constant (sec. 1); preamp gain 200; band pass filter (eq. 3); demodulator (eq. 4); and low pass filter (eq. 5). The frequency dependence is plotted in figures 16 and 17. The DC gains are tabulated below. Since they are based upon nominal gyro parameters, it is necessary to calibrate the system to obtain the actual values.

The output of the low pass filter is digitized with a 12 bit analog to digital converter (ADC) whose input range is ±5 volts.

	TGG	18 mod D	units
Electronic gain (RMS input, DC output)	14400	144000	
Measurement system gain	260000	490000	V/rad
ADC range	+19	+10.2	μrad
ADC quantization	9.4	5.0	nrad

Note: Based upon nominal gyro parameters.

Actual DC gains (based on nominal gyro parameters):

TGG	260000 V/rad
TGG electronics only	14400
18 Mod D	490000 V/rad
18 Mod D electronics only	14400

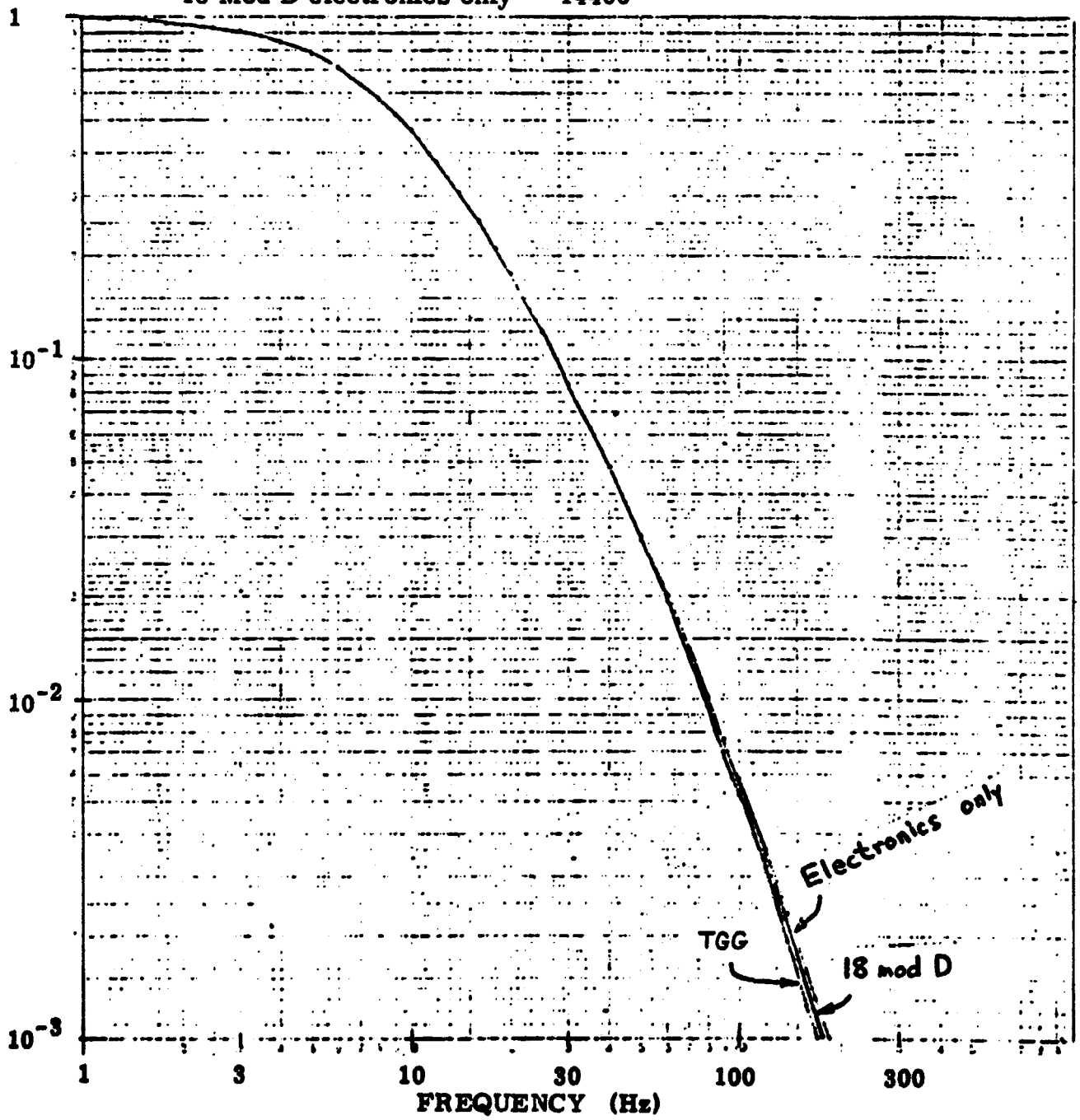

Fig. 16 Gain of Noise Measurement System, Normalized to 1 at DC

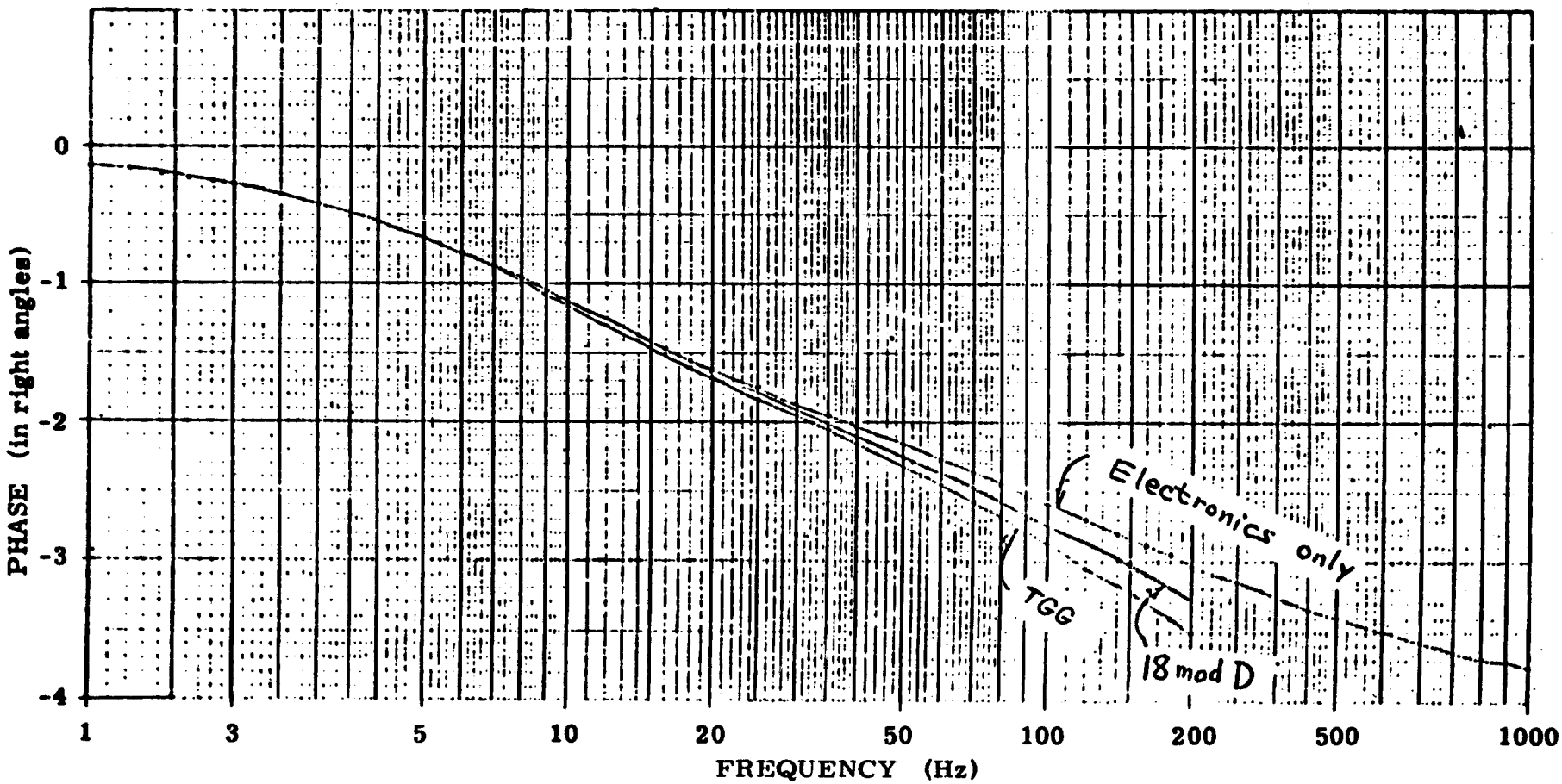

Fig. 17 Phase Response of Noise Measurement System

CHAPTER 5
POWER SPECTRAL DENSITY TECHNIQUES

This paper is an introduction to Fourier transforms and power spectral density techniques in the measurement of signals and noise. Section 1 provides the mathematical basis and includes explanations of aliasing, Fourier tranforms, power spectral density, and the fast Fourier transform. Section 2 describes the averaging which must be used when measuring the power spectral density of noise. The importance of power spectral density is explained at the end of this section. Finally, section 3 gives some helpful computer methods.

1. Mathematical Basis.

1.1. Positive and Negative Frequencies.

A signal of a single frequency f is given by

$$x(t) = a\, e^{2\pi i f t} + a^{*}\, e^{-2\pi i f t} \qquad (1)$$

The two terms in (1) are at positive and negative frequencies. The amplitudes $\underline{a}$ and $\underline{a}^{*}$ must be complex conjugates of each other in order for x(t) to be real. Equation (1) is equivalent to

$$x(t) = 2|a|\cos(2\pi f t + \phi), \quad \phi = \arg a, \qquad (2)$$

so that the use of positive and negative frequencies is just a convenient way to specify phase information. Mathematical frequencies f and -f always appear together in a signal of physical frequency f.

1.2. Sampling and Aliasing.

Let the signal

$$x(t) = e^{2\pi i f t} \tag{3}$$

be sampled at interval Δt. The sampled values are

$$x_k = x(k\Delta t) = (e^{2\pi i f \Delta t})^k . \tag{4}$$

It is seen that for any integer m, if the frequency f is replaced by $f + m/\Delta t$, the sampled values in (4) remain unchanged. In particular the two signals

$$\left.\begin{aligned} x_1(t) &= \sum_m \left(a_m\, e^{2\pi i (f + m/\Delta t) t}\right) \\ x_2(t) &= \left(\sum_m a_m\right) e^{2\pi i f t} \end{aligned}\right\} \tag{5}$$

yield identical samples.

In order to insure a unique relation between the continuous signal and the discrete samples, we must restrict the physical frequency to the range

$$0 \leq f < \frac{1}{2\Delta t} = f_{max} . \tag{6}$$

The mathematical frequency is then restricted to the range $-f_{max} < f < f_{max}$, an interval of length $1/\Delta t$. Usually f_{max} is called the Nyquist frequency.

If frequencies greater than f_{max} are present, and the samples are processed anyway, then these higher frequencies will appear as a spurious signal below f_{max} in the manner indicated by equation (5). This distortion is called aliasing.

Example: Suppose $\Delta t = 0.01$ sec, so that $f_{max} = 50$ Hz. Suppose an $f = 60$ Hz signal is present. An integer multiple of $1/\Delta t = 100$ Hz must be added to f to bring it into the range $-50 < f < 50$. Thus $60 + (-1)(100) = -40$. So a 40 Hz spurious signal will appear. Furthermore the complex amplitude at +60Hz is added to the already existing complex amplitude at -40 Hz.

1.3. Discrete Fourier Transform.

In what follows, use will be made of the relation

$$\sum_{j=0}^{n-1} e^{2\pi i \frac{j}{n}(k-l)} = \begin{cases} n, & \text{if } k=l \mod n \\ 0, & \text{if } k\neq l \mod n . \end{cases} \tag{7}$$

Equation (7) is easily proved by representing the summands as unit vectors in the complex plane.

Let x_k, $k = 0, 1, \ldots, n-1$ be sampled values and define the Fourier transform by

$$y_j = \sum_{k=0}^{n-1} e^{-2\pi i \frac{jk}{n}} x_k . \tag{8}$$

It is seen that

$$y_{j+n} = y_j , \tag{9}$$

so that y_j is periodic in j with period n. It will sometimes be convenient to regard the range $0 \leqslant j \leqslant n-1$ as the fundamental period, and sometimes the range

$$\left.\begin{aligned} -\tfrac{n}{2}+1 \leqslant j \leqslant \tfrac{n}{2}, &\quad \text{for } n \text{ even} \\ -\tfrac{n-1}{2} \leqslant j \leqslant \tfrac{n-1}{2}, &\quad \text{for } n \text{ odd.} \end{aligned}\right\} \tag{10}$$

The inverse Fourier transform is

$$x_k = \frac{1}{n} \sum_{j=0}^{n-1} e^{+2\pi i \frac{jk}{n}} y_j . \tag{11}$$

To verify this, substitute (8) into the right hand side of (11). Using (7), the right hand side simplifies to x_k. Since (8) and (11) are linear transforms on an n-dimensional vector space whose product is the identity, they are

inverses of each other.

Equation (11) expresses the signal x(t) as a superposition of single frequency signals. If we wish to put equation (11) into the form

$$x_k = x(k\Delta t) = \frac{1}{n}\sum_j y_j\, e^{2\pi i f_j\, k\Delta t}\,, \tag{12}$$

we must have

$$f_j\, k\Delta t = \frac{jk}{n} + m_j \tag{13}$$

for some integers m_j (because the exponential function has period $2\pi i$).

$$f_j = \frac{j}{n\Delta t} + \frac{m_j}{k\Delta t} \tag{14}$$

Since f_j cannot depend upon k, we must have $m_j = mk$, with m an integer, and so

$$f_j = \frac{j}{n\Delta t} + \frac{m}{\Delta t}\,. \tag{15}$$

According to the restriction (6), we set m = 0, and in (12) sum j over the range given by (10).

Using the notations

$$\Delta f = \frac{1}{n\Delta t}\,, \tag{16}$$

$$y(j\Delta f) = y_j\,, \tag{17}$$

we put (12) in the form

$$x(t) = \frac{1}{n}\sum_j y(j\Delta f)\, e^{2\pi i (j\Delta f)\, t}\,, \tag{18}$$

which is manifestly a superposition of single frequency signals. The summation range is given by (10), and is approximately $-n/2 < j < n/2$. Therefore the maximum frequency is $(n/2)/(n\Delta t) = f_{max}$, in agreement with (6).

1.4. Degrees of Freedom.

Reality of x_k requires

$$y_{-j} = y_j^* \tag{19}$$

and in particular y_0 is real. Periodicity of y_j, equation (9), requires that $y_{n/2}$ be real.

The sampled values are n real numbers. The Fourier coefficients y_j also have n degrees of freedom: y_0, which is real; if n is odd, then (n-1)/2 complex numbers y_j for $1 \leqslant j \leqslant (n-1)/2$; if n is even, then n/2-1 complex numbers y_j for $1 \leqslant j \leqslant n/2-1$ and $y_{n/2}$, which is real.

It is easily seen why $y_{n/2}$ has one rather than two degrees of freedom. At this frequency the sampling occurs at 180^0 phase intervals. If t = 0 is one of the sample times, then the signal $\sin(2\pi ft)$ will always be zero when it is sampled.

1.5. Power Spectral Density.

The power in the signal x(t) is defined by

$$P = \frac{1}{T}\int_0^T x(t)^2\,dt \approx \frac{1}{n\Delta t}\sum_{k=0}^{n-1} x(k\Delta t)^2\,\Delta t \tag{20}$$

$$= \frac{1}{n}\sum_{k=0}^{n-1} x_k^2 . \tag{21}$$

Substitute for x_k from (11) and use (7) to obtain

$$P = \frac{1}{n^2}\sum_j |y_j|^2 \tag{22}$$

$$= \frac{1}{n^2\Delta f}\sum_j |y(j\Delta f)|^2\,\Delta f . \tag{23}$$

For a continuous frequency domain, the power spectral density is defined by

$$P = \int_{f_{min}}^{f_{max}} PSD(f)\,df . \tag{24}$$

If we now regard (23) be being summed over the range (10) and regard it as the discrete approximation to (24), we have

$$PSD(j\Delta f) = \frac{1}{n^2 \Delta f} \left(|y_j|^2 + |y_{-j}|^2 \right), \qquad (25)$$

for $j \neq 0, n/2$. Using (19) and (16),

$$PSD(j\Delta f) = \begin{cases} \frac{2\Delta t}{n} |y_j|^2, & j \neq 0, \frac{n}{2} \\ \frac{\Delta t}{n} |y_j|^2, & j = 0, \frac{n}{2} \end{cases} \qquad (26)$$

The cases $j = 0$ or $n/2$ are special since there is only one degree of freedom at frequencies $f = 0$ and $f = f_{max}$ compared to the usual two degrees of freedom at other frequencies. The case $f = f_{max}$ can be ignored because if the component at this frequency is not negligible, then there will usually be non-negligible components at slightly higher frequencies, and these will cause aliasing. The case of zero frequency may or may not be important in particular applications.

1.6. Filtered Signals.

If the signal x(t) is the input to a linear system with transfer function G(s), and if u(t) is the output, then u(t) has a Fourier transform $V(f)$. It is clear that the relations between the two Fourier transforms and the two power spectral densities are

$$V(f) = G(2\pi i f)\, y(f), \qquad (27)$$

$$PSD_u(f) = |G(2\pi i f)|^2 \, PSD_x(f). \qquad (28)$$

Example: An integrating gyroscope provides a direct readout of angle. By use of an analog torque to balance loop, we can get a readout of angular velocity. The power spectral density of the instrument noise is given in the former case as $PSD_\theta(f)$ in units of radian ^{2}/Hz, and in

the latter case as $PSD_\omega(f)$ in units of $(\text{radian/sec})^2/\text{Hz}$. These two representations of the gyroscope noise are related by

$$PSD_\omega(f) = (2\pi f)^2 \, PSD_\theta(f).$$

1.7. RMS Values.

From (21), (22) and (25)

$$\chi_{RMS}^2 = P = \sum_{0 \le j\Delta f \le f_{max}} PSD(j\Delta f)\, \Delta f. \qquad (29)$$

If x(t) is filtered with an ideal band pass filter which only passes frequencies between f_1 and f_2, then it follows from (28) that the RMS value of the output is

$$\chi_{RMS}(f_1,f_2)^2 = \sum_{f_1 \le j\Delta f \le f_2} PSD(j\Delta f)\, \Delta f. \qquad (30)$$

In the continuous case,

$$\chi_{RMS}(f_1,f_2)^2 = \int_{f_1}^{f_2} PSD(f)\, df. \qquad (31)$$

By allowing f_1 and f_2 to become close together, we see the physical significance of the power spectral density: PSD(f) Δf is the amount of power present in the signal in a bandwidth Δf about frequency f.

If x(t) is measured in units X (e.g. volts), then the power spectral density is measured in units X^2/Hz.

1.8. Effects of Finite Frequency Resolution.

We can think of a signal as possessing a power spectral density, which we want to measure. If the duration of the test is $T = n\Delta t$, then the measurement has a frequency resolution $\Delta f = 1/T$.

If the signal has a broad band power spectrum, then for sufficiently small Δf, a further decrease will not change the measured values of PSD(f) On the other hand, if the signal contains a finite amount of power at a single frequency f_0, then the true power spectral density must have an impulse function at f_0 because the integral in (31) takes a jump in value when one of the limits of integration passes through f_0. In this case, as Δf decreases, the measured PSD(f) will increase indefinitely in a decreasing neighborhood of f_0.

As an example, let us consider a single frequency signal

$$x(t) = a\, e^{2\pi i f_0 t} + a^*\, e^{-2\pi i f_0 t} \tag{32}$$

Let j_0 be the nearest integer to $f_0/\Delta f$. Then we expect that the significant values of y_j will occur for $j \approx \pm j_0$. Assume that $j_0 \gg 1$ and $n/2 - j_0 \gg 1$, which means that the positive and negative frequency parts are separated by a large multiple of Δf. A straightforward derivation then yields.

$$PSD(j\Delta f) \approx \frac{2a^2}{\Delta f} \frac{\sin^2\left(\pi\left(\frac{f_0}{\Delta f} - j\right)\right)}{\pi^2\left(\frac{f_0}{\Delta f} - j\right)^2}. \tag{33}$$

If f_0 is not an integer multiple of Δf, then the measured power spectral density will be spread out with side lobes falling off as $(j - j_0)^{-2}$.

1.9. Hanning Window

The $(j - j_0)^{-2}$ spread is characteristic of a discontinuity in the data. From a mathematical point of view the data x_k are periodic with period n, and therefore there is an end point discontinuity between x_{n-1} and $x_n = x_0$.

The end point discontinuity can be eliminated by multiplying the data by a window function which smoothly falls to zero at the end points. The Hanning window is

$$W_k = \sqrt{\frac{2}{3}}\left(1 - \cos\frac{2\pi k}{n}\right) \tag{34}$$

the factor $\sqrt{2/3}$ is needed to keep the average power in $u_k = w_k x_k$ the same as in the original x_k.

It is usually easier to apply the Hanning window in the frequency domain. If z_j and v_j are the Fourier transforms of w_k and u_k respectively, then for an arbitrary window

$$v_j = \sum_{\ell=0}^{n-1} z_\ell\, y_{j-\ell}, \tag{35}$$

and for the Hanning window

$$v_j = \sqrt{\frac{2}{3}}\left(y_j - \frac{1}{2}\left(y_{j-1} + y_{j+1}\right)\right). \tag{36}$$

In (35) and (36) the periodicity of the Fourier transform is implicitly used.

Considering again the signal in (32) and the same approximations used above, we get for the power spectral density with Hanning

$$PSD(j\Delta f) \approx \frac{4a^2}{3\Delta f}\,\frac{\sin^2\left(\pi\left(\frac{f_0}{\Delta f} - j\right)\right)}{\pi^2\left(\frac{f_0}{\Delta f} - j\right)^2\left(\left(\frac{f_0}{\Delta f} - j\right)^2 - 1\right)^2}. \tag{37}$$

Now the side lobes fall off as $(j-j_0)^{-6}$. This faster fall off is a consequence of the continuity of the signal and its first derivative at the end points.

The price paid for smaller side lobes is a more spread out center lobe.

1.10 The Fast Fourier Transform (FFT).

The FFT is an algorithm discovered by Cooley and Tukey (Mathematics of Computation, Vol. 19, 1965, p. 297), which enables the Fourier transform to be computed in a reasonable amount of time. It will be assumed that n is a power of 2.

Let x_k, $k = 0, \ldots, n-1$ be the given sequence, whose Fourier transform y_j, $j = 0, \ldots, n-1$ is sought. Let x_k, $k = 0, \ldots n/2-1$ be the sequence of even terms, $x'_k = x_{2k}$, and let y'_j, $j = 0, \ldots, n/2-1$ be its Fourier transform. Let x''_k, $k = 0, \ldots, n/2-1$ be the sequence of odd terms, $x''_k = x_{2k+1}$, and let y''_j, $j = 0, \ldots, n/2-1$ be its Fourier transform.

From the definition (8),

$$y_j = \sum_{k=0}^{n/2-1} e^{-2\pi i \frac{j(2k)}{n}} x_{2k} + \sum_{k=0}^{n/2-1} e^{-2\pi i \frac{j(2k+1)}{n}} x_{2k+1}$$

$$= \sum_{k=0}^{n/2-1} e^{-2\pi i \frac{jk}{n/2}} x'_k + e^{-2\pi i \frac{j}{n}} \sum_{k=0}^{n/2-1} e^{-2\pi i \frac{jk}{n/2}} x''_k$$

$$= y'_j + e^{-2\pi i \frac{j}{n}} y''_j . \qquad (38)$$

When $j \geq n/2$, y'_j and y''_j are defined by their periodicity, equation (9), where here the period is $n/2$. Equation (38) can be written as

$$\left.\begin{aligned} y_j &= y'_j + e^{-2\pi i \frac{j}{n}} y''_j \\ y_{j+\frac{n}{2}} &= y'_j - e^{-2\pi i \frac{j}{n}} y''_j \end{aligned}\right\} \qquad (39)$$

for $j = 0, 1, \ldots, n/2-1$.

To obtain y_j' and y_j'', apply equations (39) recursively, with n/2 in place of n, y'_j or y''_j in place of y_j and appropriate subsequences in place of y'_j and y''_j. Since n is a power of 2, this recursion can be applied until n=1, where the Fourier transform of a single number is that same number.

Similar algorithms can be derived for prime numbers other than 2. For each distinct prime factor of n, a separate set of equations is needed, (39) being the set for the prime number 2. However, the FFT algorithm is most efficient when n is a power of 2.

Computing the transform directly from (8) as a matrix product requires n^2 multiplications. Using the FFT, equation (39), requires $n \log_2 n$ multiplications. If we take as a typical case n=2048 and assume 1 msec to do a complex multiplication, then use of the FFT reduces the computation time from 70 minutes to 23 seconds.

2. Analysis of Noise.

The values of the signal at particular instants of time are random and satisfy some probability distribution. If the noise has non-zero mean, lump this mean with the non-random part of the signal.

We assume the noise is stationary, i.e., that the statistical properties are unchanged by a shift in time.

2.1. Gaussian Noise.

The following analysis is rendered simple by assuming that the noise is Gaussian. The values of the n samples $x_0, x_1, \ldots, x_{n-1}$ are given by a Gaussian joint probability distribution. Since the Fourier transform, equation (8), is linear, the real and imaginary parts of all the y_j also have a Gaussian joint probability distribution.

For a fixed frequency $j\Delta f$ examine the two-dimensional probability distribution of y_{jR} and y_{jI}, the real and imaginary parts of y_j. It is Gaussian with covariance matrix.

$$C = \begin{bmatrix} \sigma_R^2 & r\sigma_R\sigma_I \\ r\sigma_R\sigma_I & \sigma_I^2 \end{bmatrix}. \qquad (40)$$

For a time shift corresponding to a phase shift ϕ, y_j is multiplied by $e^{i\phi}$. This is a rotation of the y_{jR} and y_{jI} axes in the y_j plane. Matrix C is left unchanged by all such rotations of axes if and only if

$$C = \begin{bmatrix} \sigma^2 & 0 \\ 0 & \sigma^2 \end{bmatrix}. \qquad (41)$$

Thus, if the noise is stationary, the real and imaginary parts of y_j are independent.

The y_{jR}, y_{jI} probability distribution is

$$P(y_{jR}, y_{jI}) = \frac{1}{2\pi\sigma^2} \exp\left(-\frac{(y_{jR}-u_R)^2 + (y_{jI}-u_I)^2}{2\sigma^2}\right), \qquad (42)$$

where u_R, u_I are the non-random mean values. With y_{jI} held constant, the probability distribution in y_{jR} has mean u_R and variance σ^2. Therefore, using an overbar to denote mean value,

$$\overline{y_{jR}^2} = (\bar{y}_{jR})^2 + \sigma^2 = u_R^2 + \sigma^2. \qquad (43)$$

Similarly,

$$\overline{y_{jI}^2} = u_I^2 + \sigma^2. \qquad (44)$$

Adding (43) and (44),

$$\overline{|y_j|^2} = u_R^2 + u_I^2 + 2\sigma^2. \qquad (45)$$

Now, u_R and u_I depend upon the relative phase between the signal and the sample times.

$$u_R = u\cos\phi, \qquad u_I = u\sin\phi,$$

$$\overline{|y_j|^2} = u^2 + 2\sigma^2. \tag{46}$$

The quantity $|y_j|^2$ is a random variable with mean given by (46). To obtain its standard deviation, consider for simplicity the two limiting cases $u \gg \sigma$ and $u = 0$.

In the former case, use the techniques of error analysis.

$$\Delta(|y_j|^2) = 2y_{jR}\,\Delta y_{jR} + 2y_{jI}\,\Delta y_{jI}. \tag{47}$$

Combine the errors as independent and use $y_{jR} \approx u_R$, $y_{jI} \approx u_I$, $\Delta y_{jR} = \Delta y_{jI} = \sigma$.

$$\frac{\Delta(|y_j|^2)}{|y_j|^2} = \frac{2(u_R^2 + u_I^2)^{\frac{1}{2}}\,\sigma}{u^2} = \frac{2\sigma}{u}. \tag{48}$$

If $u = 0$, then from (26), $|y_j|^2$ has a chi-square distribution with 2 degrees of freedom, and this distribution is

$$P(z) = \begin{cases} 0 & , \ z < 0 \\ \frac{1}{2\sigma^2}\, e^{-\frac{z}{2\sigma^2}} & , \ z > 0. \end{cases} \tag{49}$$

The mean and standard deviation are both equal to $2\sigma^2$.

Summary of this section: If, at a given frequency f, the signal consists of a non-random component of amplitude u and a Gaussian random component having standard deviation σ in each of its two degrees of freedom, and if the power spectral density, PSD(f), is calculated by equation (26), then PSD(f) is a random variable for which the ratio (standard deviation)/(mean) has the value 1 for $u \ll \sigma$, the value $2\sigma/u$ for $u \gg \sigma$, and varies smoothly in between.

Conclusion of this section: In order to obtain a reliable estimate of PSD(f), it is necessary to make repeated measurements and average. If N measurements are averaged, the standard deviation in the estimate will be reduced by a factor of $\sqrt{N}$. If we want the ratio (standard deviation) /(mean) for the estimate to be ϵ, then in the most pessimistic case (u=0), we must have

$$N = \frac{1}{\epsilon^2} \quad . \tag{50}$$

Note that this conclusion depends to some extent on the assumption of Gaussian noise.

2. 2. Importance of Power Spectral Density in the Description of Noise in Linear Systems.

Power spectral density is an essential tool in describing noise in linear systems. If we know the PSD of the input noise, equation (28) gives the output noise PSD, and equation (31) gives the RMS value of the noise. Alternatively, if we know the output noise PSD and the transfer function, then we can calculate the input noise PSD. When independent noise sources are added, the PSDof the sum noise is conveniently the sum of the individual PSD's.

The significance of the PSD is that it carries the necessay frequency dependent information. If we only knew the RMS input noise to a frequency depdendent linear system, we would be unable to compute the RMS output noise.

Example: A resistance R and capacitance C are in parallel. What is the RMS thermal noise across the parallel combination?

The resistance generates thermal noise with power spectral density

$$PSD_{in}(f) = 4kTR$$

in units of volt^2/Hz. Boltzmann constant: $k = 1.38 \times 10^{-23}$ joule/$^\circ$K. The gain of the system is

$$G(s) = \frac{1}{1+\tau s}, \quad \tau = RC$$

The output PSD is

$$PSD_{out}(f) = \frac{4kTR}{|1+2\pi i\tau f|^2} = \frac{4kTR}{1+(2\pi\tau f)^2}$$

The RMS output noise is

$$V_{RMS}^2 = \int_0^\infty \frac{4kTR}{1+(2\pi\tau f)^2}\,df = 4kTR\,\frac{\pi}{4\pi\tau} = \frac{kT}{C}.$$

For T = 300 $^\circ$K, C = 1μF, this becomes V_{RMS} = 65 nanovolts.

3. Computational Techniques.

The most important computational technique is the FFT, described in section 1.10.

3.1. Efficient Use of Memory.

The FFT algorithm can be programmed in such a way that each time equation (39) is applied, the new values are stored back in the same memory locations occupied by the old values. To perform an FFT on a sequence of length n, one needs 2n words of memory: n for the data (real part of x_k), n of zeroes (imaginary part of x_k). One also needs n/2 words to hold the power spectral density and n/4 words for a table of sines.

By separating equation (39) into its real and imaginary parts, one can carry out the FFT algorithm using only n words of memory. Furthermore, this can also be programmed so that at each step the same memory locations are reused.

Another computational trick allows two Fourier transforms to be taken in the same FFT operation. From (19), if x_k are real, the real part of y_j is an even function of j and the imaginary part of y_j is an odd function of j. Similarly if x_k are imaginary, the real part of y_j is an odd function of j and the imaginary part of y_j is an even function of j. Therefore, two sets of data can be stored as the real and imaginary parts of x_k, and their respective Fourier transforms can be separated at the end of the calculation.

Suppose the two sets of data are independent sets of samples of the same signal. Applying equation (26) for $j \neq 0, n/2$, we see that the real data gives

$$PSD_j = \frac{2\Delta t}{n}\left[\left(\frac{y_{jR} + y_{-jR}}{2}\right)^2 + \left(\frac{y_{jI} - y_{-jI}}{2}\right)^2\right], \qquad (51)$$

and the imaginary data gives

$$PSD_j = \frac{2\Delta t}{n}\left[\left(\frac{y_{jR} - y_{-jR}}{2}\right)^2 + \left(\frac{y_{jI} + y_{-jI}}{2}\right)^2\right]. \qquad (52)$$

If these two measurements are averaged, we get, after some easy algebra,

$$PSD_j = \frac{\Delta t}{2n}\left(|y_j|^2 + |y_{-j}|^2\right). \qquad (53)$$

This allows the power spectral density averaging technique to be done two at a time.

3.2. Digital Filtering to Reduce Aliasing.

Suppose the analog to digital converter can convert at time interval ΔT, but we want a sample time

$$\Delta t = r\ \Delta T\ . \tag{54}$$

Instead of letting the computer to idle for time Δt, we can average data. Thus we program a digital filter whose input is $x_k = x(k\Delta T)$ and whose output is

$$u_j = u(j\Delta t) = \frac{1}{r} \sum_{k=0}^{r-1} x_{rj+k}\ . \tag{55}$$

If the input is at frequency f,

$$x_k = e^{2\pi i f (k\Delta T)}\ , \tag{56}$$

then the output is

$$u_j = \left\{ e^{\pi i (1-\frac{1}{r}) f\Delta t}\ \frac{\sin(\pi f \Delta t)}{r \sin\left(\frac{\pi f \Delta t}{r}\right)} \right\} e^{2\pi i f (j\Delta t)} \tag{57}$$

The filter output covers a frequency range

$$f < \frac{1}{2\Delta t}\ , \tag{58}$$

and because of aliasing, this frequency f receives components from the set of frequencies

$$f_1 = \left| f + \frac{m}{\Delta t} \right|\ , \tag{59}$$

where m is an integer. If the components at these different frequencies are uncorrelated, then the power spectral densities are additive, but with transfer function weighting given by (57).

$$PSD_{out}(f) = \sum_{m=-\infty}^{\infty} \left(\frac{\sin\left(\pi \left| f + \frac{m}{\Delta t} \right| \Delta t\right)}{r \sin\left(\frac{\pi}{r} \left| f + \frac{m}{\Delta t} \right| \Delta t\right)} \right)^2 PSD_{in}\left(\left| f + \frac{m}{\Delta t} \right| \right)$$

$$= \sum_{m=-\infty}^{\infty} \frac{\sin^2(\pi f \Delta t)}{r^2 \sin^2\left(\frac{\pi}{r}(f\Delta t + m)\right)} PSD_{in}\left(\left| f + \frac{m}{\Delta t} \right| \right). \quad (60)$$

In the limit $r \to \infty$, $\Delta T \to 0$, Δt held constant, we get

$$PSD_{out}(f) = \sum_{m=-\infty}^{\infty} \frac{\sin^2(\pi f \Delta t)}{(\pi f \Delta t)^2} PSD_{in}\left(\left| f + \frac{m}{\Delta t} \right| \right). \quad (61)$$

Although this simple digital filter does not do a terrific job of reducing aliasing, it is much better than none at all. A more complicated filter would slow down the computer and require ΔT to be larger. Alternatively, a hardware digital filter could be constructed.

CHAPTER 6

TEST RESULTS

1. 18 IRIG Mod D Tests

Two 18 IRIG Mod D gyros were set up in a back-to-back configuration as shown schematically in Fig. 1. A power spectral density (PSD) was determined for each gyro, as well as for the difference output. These results are shown in Fig 18-20.

The magnitudes of the PSD's determined were much larger than expected. The prime source of the noise appeared to be in the gyro wheel. Substantial noise also coupled from the magnetic suspension.

The noise coupled from ground motion would be expected to cancel in the difference output. However this output was comparable in size to those obtained with the individual gyros, indicating that any noise contribution from the ground was masked by the random noise emanating from the gyros.

Fig.21 shows the PSD obtained with the input to the gyro electronics shorted. The noise is well below that measured with the gyros and has an RMS value of approximately 1.5 milli-arcseconds.

2. TGG Test Results at Draper Lab

The TGG was tested at Draper Lab using an electronics design patterned after that used with the 18 IRIG. With the input to the electronics shorted the equivalent TGG angle noise is presented in Fig. 22. The noise level is somewhat lower than that obtained for the 18 IRIG, having an RMS value of approximately 1 milli-arcsecond over a frequency band of 0.01-10hz. The difference is due primarily to the higher TGG SG sensitivity. Fig. 23 presents a composite PSD obtained for the TGG over the band from approximately 0.0025 to 10 Hz. The RMS noise over the total band is 12 milli-arcseconds.

3. LST/CMG Tests at Martin Company

LST/CMG tests at Martin Company were limited to TGG noise measurements on one of the Martin test piers. After the initial setup

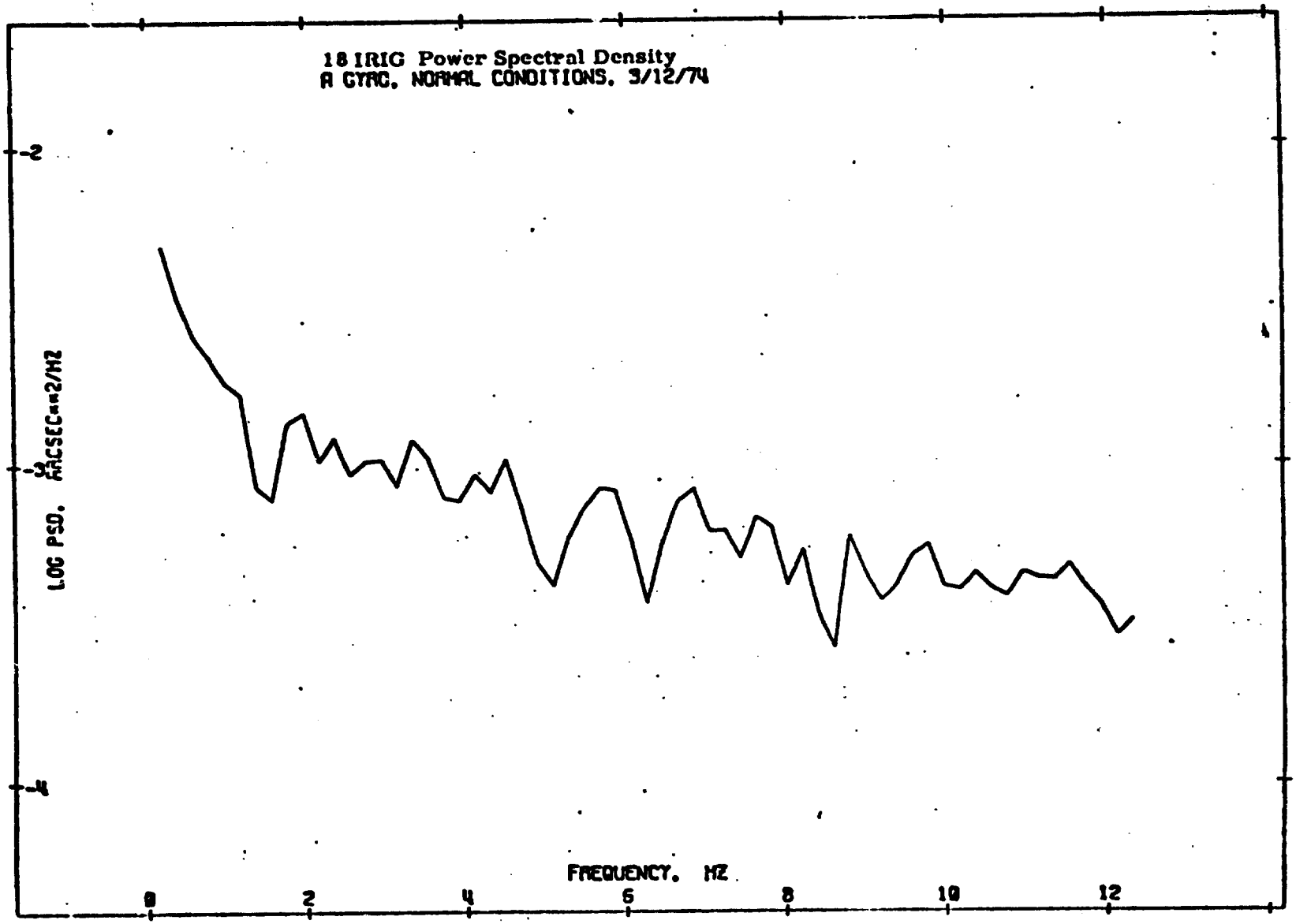

Fig. 18 18 Irig Power Spectral Density, A Gyro, Normal Conditions

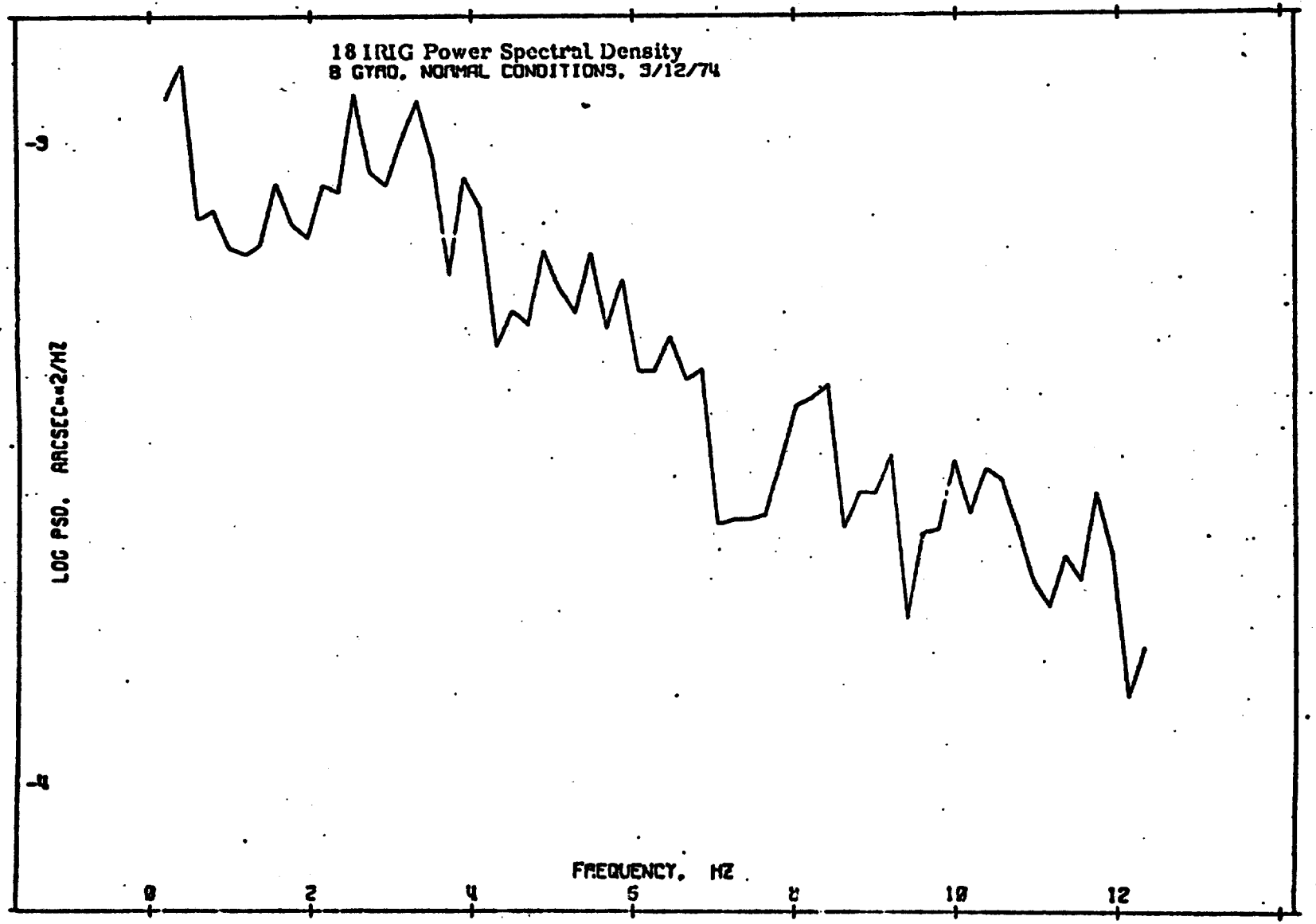

Fig. 19 18 Irig Power Spectral Density, B Gyro, Normal Conditions

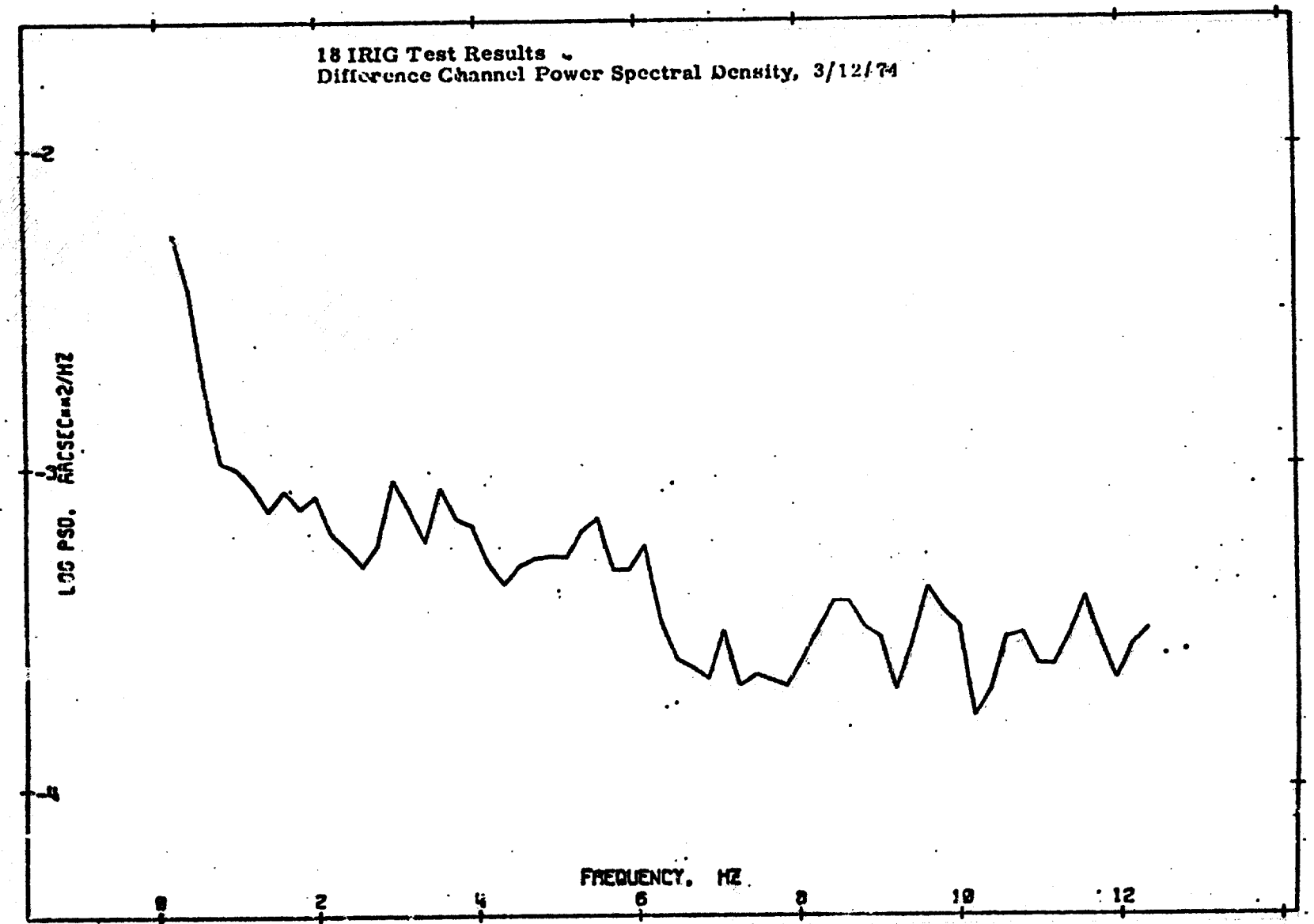

Fig. 20 18 Irig Test Results, Difference Channel Power Spectral Density

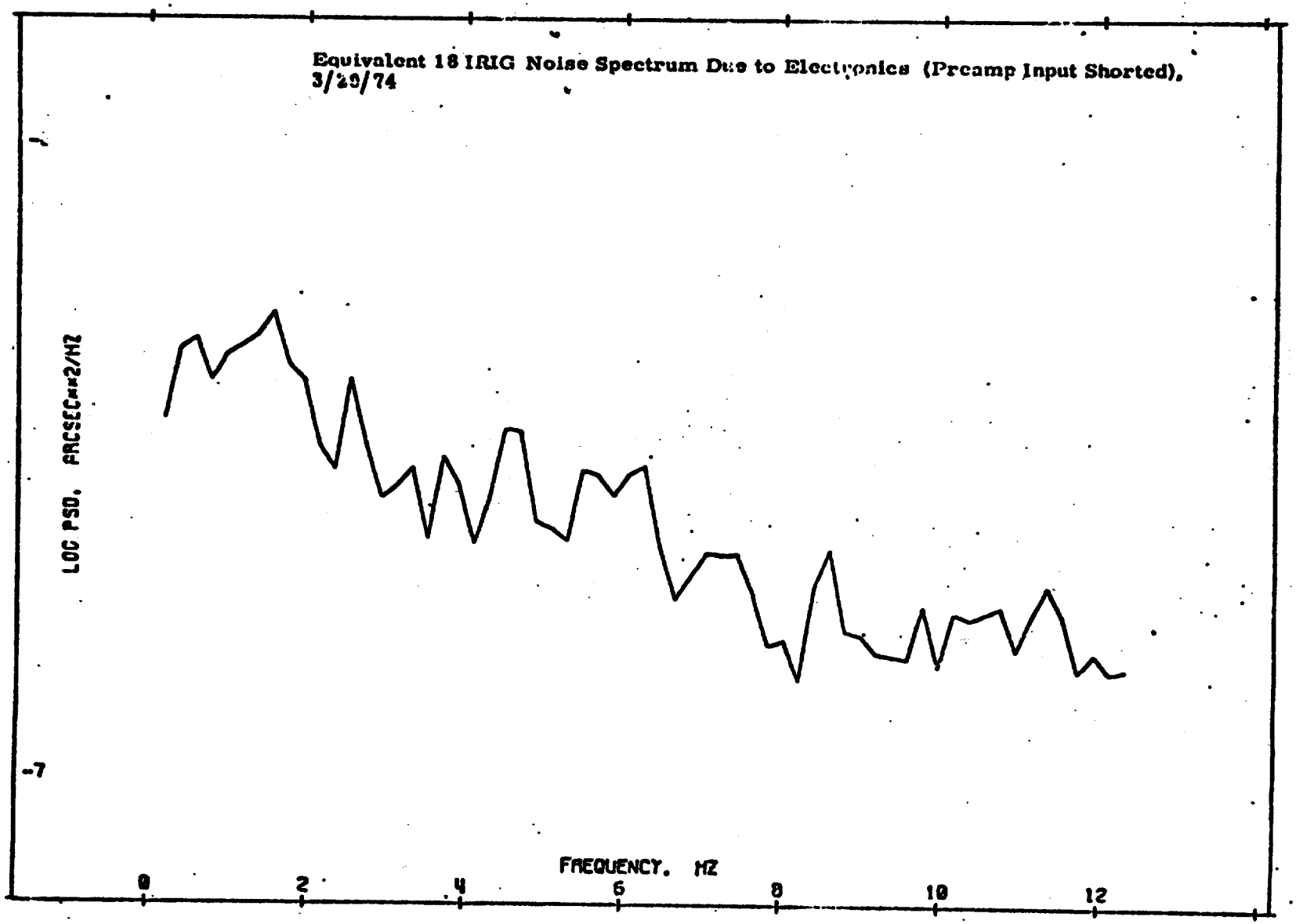

Fig. 21 Equivalent 18 Irig Noise Spectrum Due to Electronics (Preamp Input Shorted)

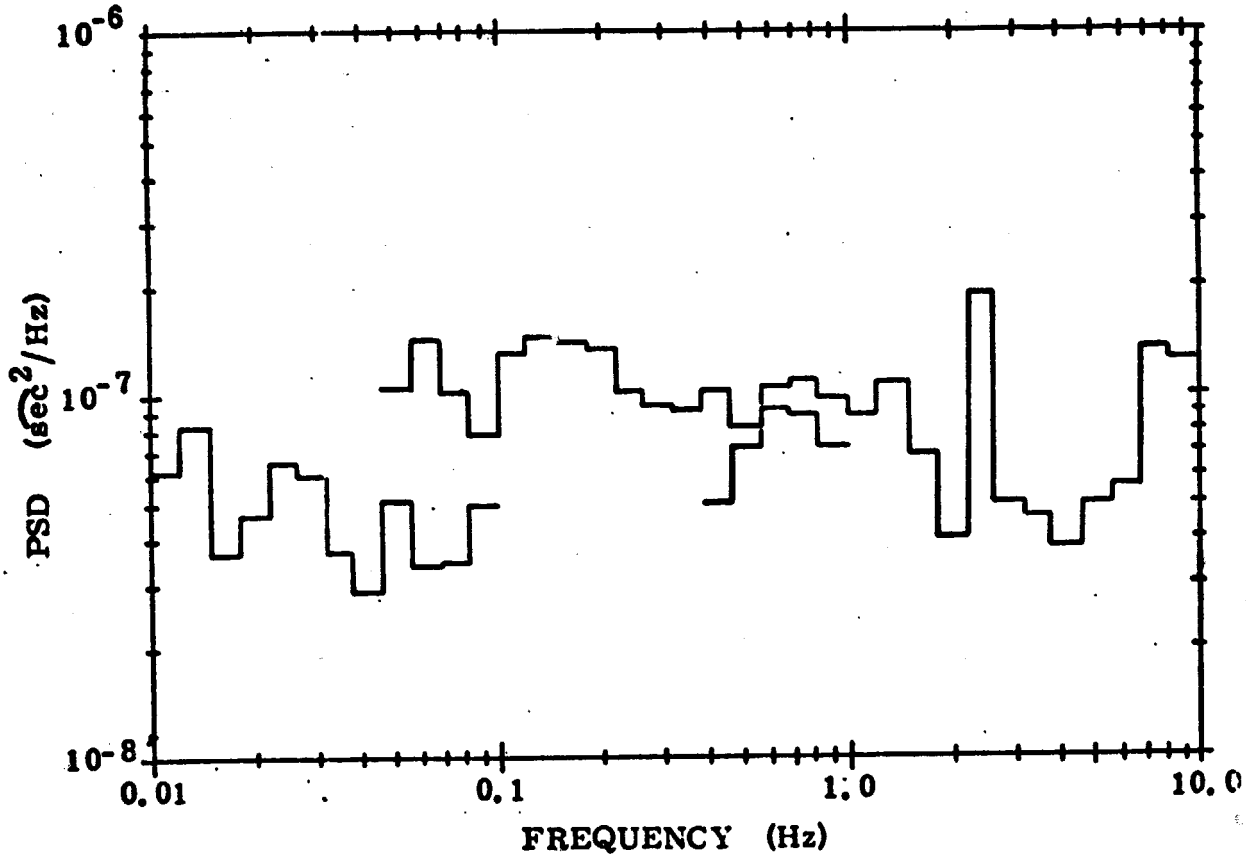

Fig. 22 Equivalent TGG Noise Spectrum Due To Electronics (Preamp Input Shorted)

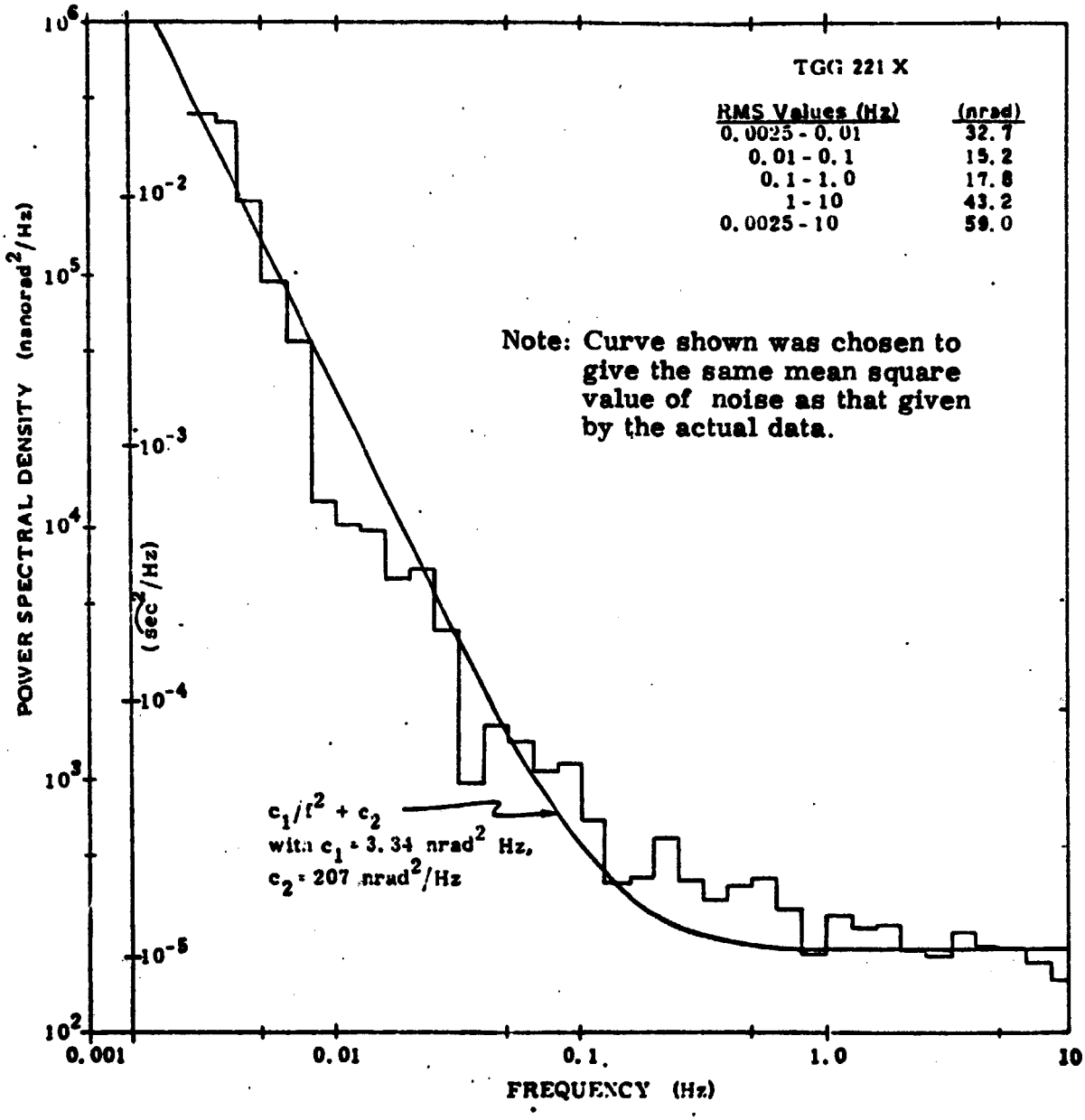

Fig. 23 Power Spectral Density (CSDL Data 3/21/75)

of equipment the TGG was position IA vertical and stabilized with constant dc current applied to the gyro torquers. Power spectral density measurements were made over a frequency range from approximately 0.05 Hz to 10 Hz (Fig. 24, 25). A composite PSD graph with averaging over discrete frequency bands is shown in Fig. 26 . The RMS noise over the band from 0.05 - 10 Hz is approximately 8 milli-arcseconds.

During the contract extension period, data taken on the test pier with IA horizontal was recorded on magnetic tape and later was reduced at Draper Laboratory. Fig. 27 presents a computed PSD over the frequency range from approximately 0.05 to 10 Hz. Some averaging was performed resulting in a more accurate, smoother plot. The data is in good agreement with that shown in Fig. 26 .

The occasional spikes shown in the plot are believed due to gyro temperature controller noise. The RMS noise for the band shown is 0.009 arc second. Without including the larger spikes the RMS noise from 0.05 to 10 Hz is 0.005 arc second.

Fig. 28 presents a PSD obtained from the same data tape for the frequency range from $\sim$ 0.01 Hz to 0.5 Hz. The results agree well with data taken at Draper Laboratory (Fig. 23).

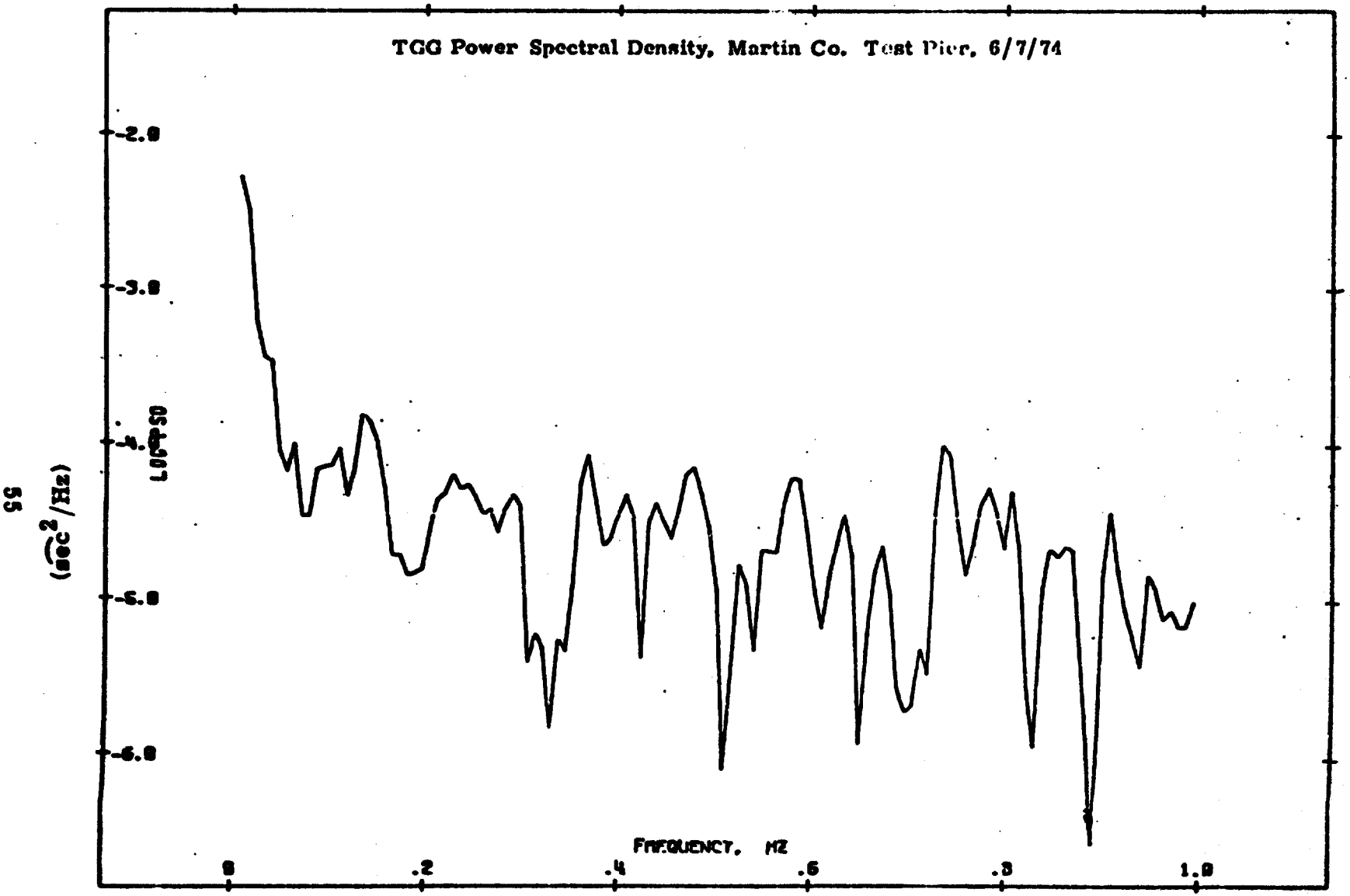

Fig. 24 TGG Power Spectral Density, Martin Co. Test Pier

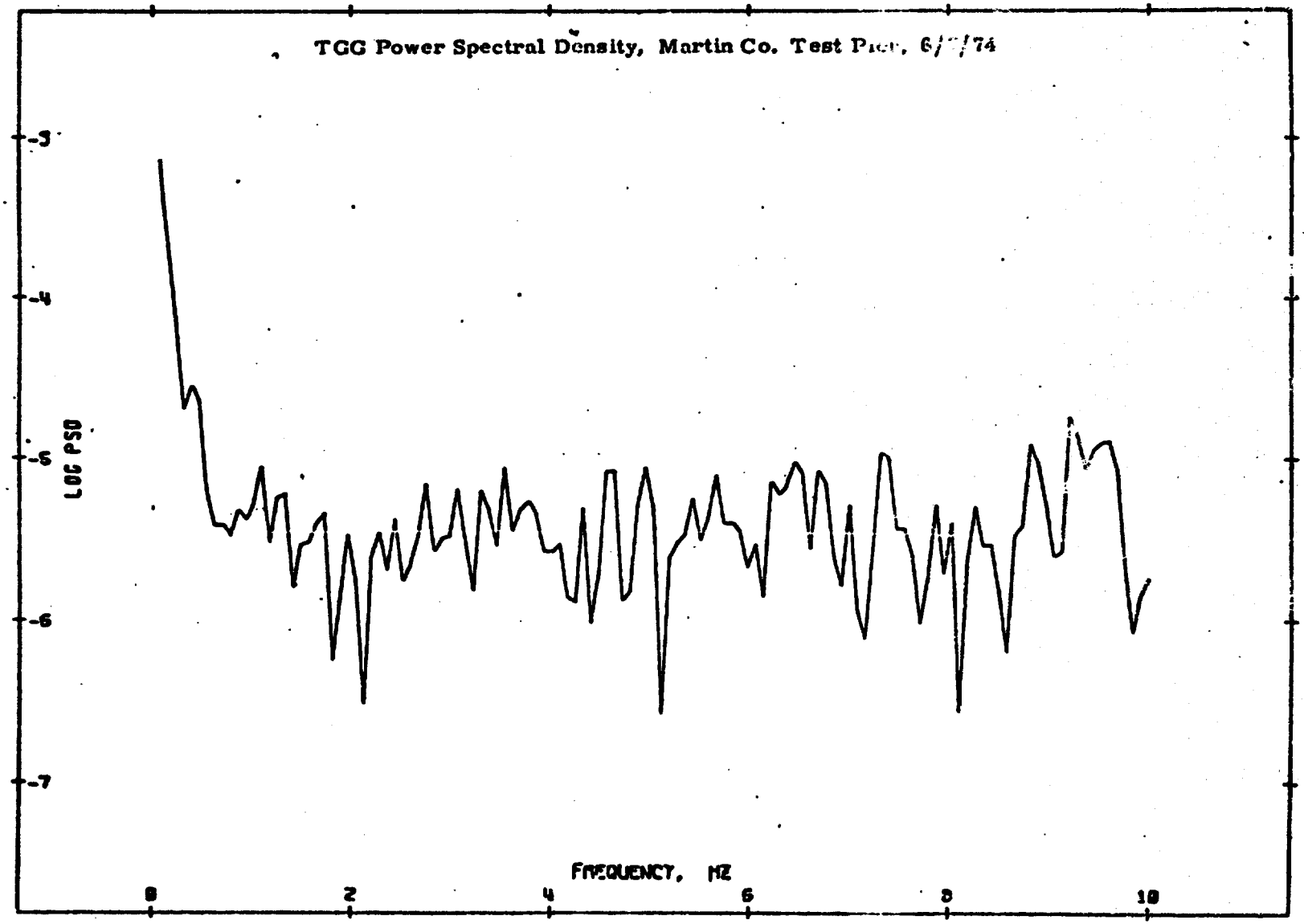

Fig. 25 TGG Power Spectral Density, Martin Co. Test Pier

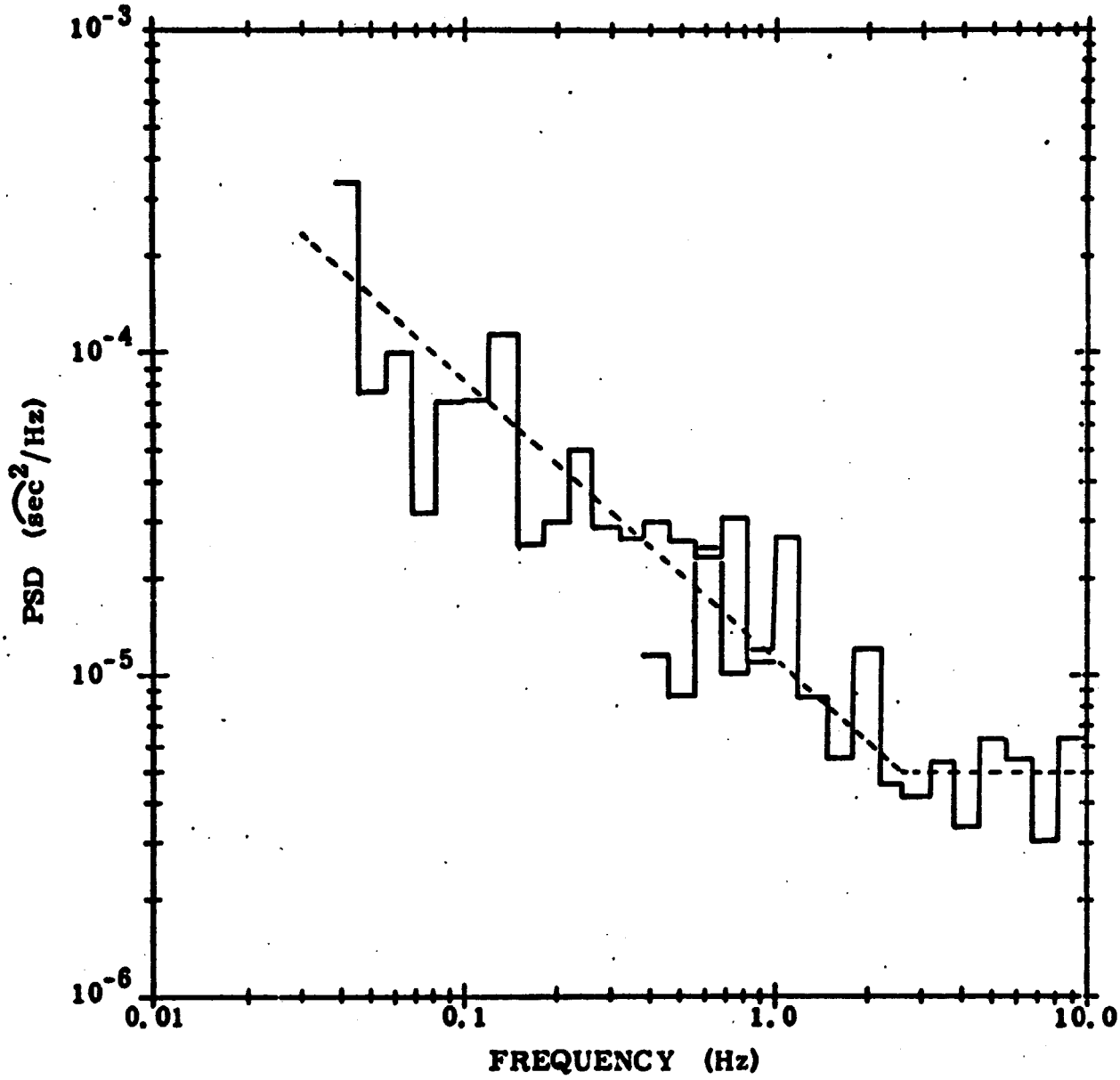

Fig. 26 TGG 221x Power Spectral Density
IGL Test Pier, Martin Company
(IA vertical)

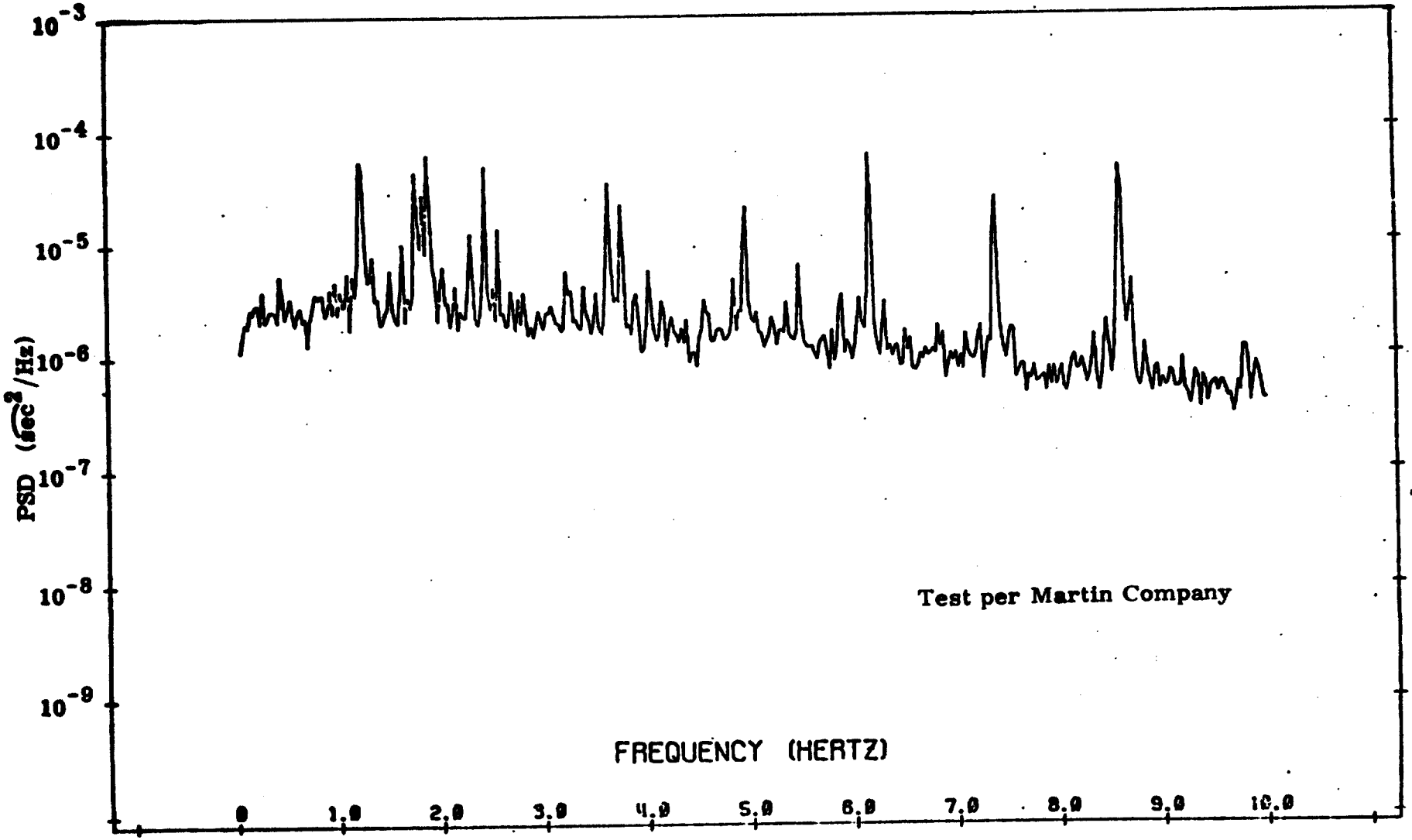

Fig. 27 TGG Power Spectral Density - High Frequency (11-4-74)

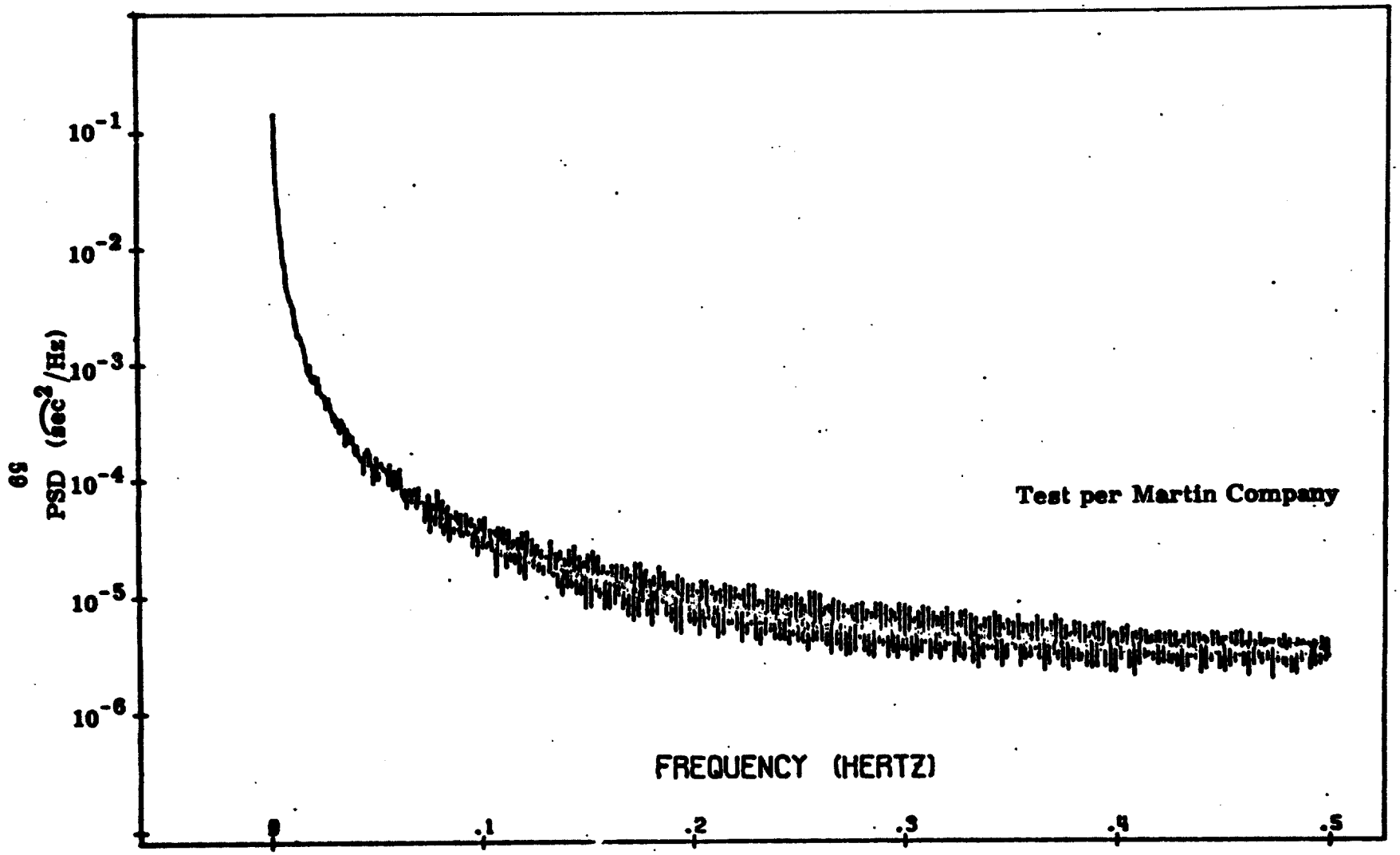

Fig. 28 TGG Power Spectral Density - Low Frequency (11-4-74)

CHAPTER 7

CONCLUSIONS

Based on Draper Laboratory data (Fig. 23) the TGG noise over a frequency band from 0.0025 to 10 Hz is 12 milli-arcsecond. Additional data recorded with the TGG on the test pier at Martin Company and later processed at Draper Laboratory shows that the true gyro noise in a seismicly quiet environment may be somewhat less than this value: i.e., 0.009 arc second over the 0.0025 - 10 Hz band.

The test results showed that the TGG is compatible with LST requirements, though the frequency band over which the gyro would maintain control would need to be reduced if a maximum 0.005 arc second RMS noise were required.

To reduce the gyro noise to an RMS value near one milli-arcsecond will require changes in the instrument; i.e. shrouding the wheel and/or making changes in instrument gain and suspension mechanization to minimize output axis coupling from the wheel and other instrument error torques.

BIBLIOGRAPHY

1. "Third Generation Gyro Procedures and Specifications", Inertial Gyro Group, GY-1000, vol. 1, sec. 2.4.
2. "18 IRIG mod D Design Specifications", FBM/Inertial Components, IC-1627, 12 September 1972.
3. "Linear Integrated Circuits", National Semiconductor Corp.
4. "Linear Applications", National Semiconductor Corp.
5. "Operational Amplifiers, Design and Applications", Burr-Brown Corp., pub. by McGraw-Hill.